# Simulating the Holocene evolution of Ryder Glacier, North Greenland

Jamie Barnett[1,2], Felicity A. Holmes[1,2], Joshua Cuzzone[3], Henning Åkesson[4], Mathieu Morlighem[5], Matt O'Regan[1,2], Johan Nilsson[2,6], Nina Kirchner[2,7,8], and Martin Jakobsson[1,2]

[1]Department of Geological Sciences, Stockholm University, Sweden
[2]Bolin Centre for Climate Research, Stockholm University, Sweden
[3]Joint Institute for Regional Earth System Science and Engineering, University of California, Los Angeles
[4]Department of Geosciences, University of Oslo, Norway
[5]Department of Earth Sciences, Dartmouth College, USA
[6]Department of Meteorology, Stockholm University, Sweden
[7]Department of Physical Geography, Stockholm University, Sweden
[8]Tarfala Research Station, Stockholm University, Sweden

**Correspondence:** Jamie Barnett (jamie.barnett@geo.su.se)

**Abstract.** The Greenland Ice Sheet's negative mass balance is driven by a sensitivity to both a warming atmosphere and ocean. The fidelity of ice-sheet models in accounting for ice-ocean interaction is inherently uncertain and often constrained against recent fluctuations in the ice-sheet margin from the previous decades. The geological record can be used to contextualise ice-sheet mass loss and understand the drivers of changes at the marine margin across climatic shifts and previous extended warm periods, aiding our understanding of future ice-sheet behaviour. Here, we use the Ice-sheet and Sea-level System Model (ISSM) to explore the Holocene evolution of Ryder Glacier draining into Sherard Osborn Fjord, North Greenland. Our modelling results are constrained with terrestrial reconstructions of the paleo-ice sheet margin and an extensive marine sediment record from Sherard Osborn Fjord that details ice dynamics over the past 12.5 ka years. By employing a consistent mesh resolution of <1 km at the ice-ocean boundary, we assess the importance of atmospheric and oceanic changes to Ryder Glacier's Holocene behaviour. Our simulations show that the initial retreat of the ice margin after the Younger Dryas cold period was driven by a warming climate and the resulting fluctuations in Surface Mass Balance. Changing atmospheric conditions remain the first order control in the timing of ice retreat during the Holocene. We find ice-ocean interactions become increasingly fundamental to Ryder's retreat in the mid-Holocene; with higher than contemporary melt rates required to force grounding line retreat and capture the collapse of the ice tongue during the Holocene Thermal Maximum. Regrowth of the tongue during the neo-glacial cooling of the late Holocene is necessary to advance both the terrestrial and marine margins of the glacier. Our results stress the importance of accurately resolving the ice-ocean interface in modelling efforts over centennial and millennial time scales, in particular the role of floating ice tongues and submarine melt, and provide vital analogies for the future evolution of Ryder in a warming climate.

# 1 Introduction

The rate of mass loss from the Greenland Ice Sheet (GrIS) has increased fivefold between 1992 and 2020, culminating in a contribution to global mean sea-level rise of $13.59 \pm 1.27$ mm, roughly double that of the Antarctic Ice Sheet over the same period (Otosaka et al., 2023). Mass loss from Greenland can be partitioned between changes in the ice sheet's Surface Mass Balance (SMB) (Box, 2013; Fettweis et al., 2020), and fluctuations at the marine interface of tidewater glaciers that drain the ice sheet's interior, known as discharge (Enderlin et al., 2014; Mouginot et al., 2019). Rising atmospheric temperatures have been the key driver of increased ablation and runoff from the ice sheet (Box et al., 2022), while the present influence of warm Atlantic Waters (AW) has been another major driver in the retreat and acceleration of Greenland's marine outlet glaciers (Slater and Straneo, 2022). However, there is a large spatial and temporal heterogeneity in the amplitude at which both processes affect mass loss across the ice sheet (Mouginot et al., 2019). As a consequence, projections of future sea-level rise contribution from Greenland vary by an order of magnitude for high emissions scenarios (Goelzer et al., 2020). The largest uncertainties in such predictions stem from the limited ability of ice-sheet models to accurately resolve fluctuations in ice discharge from tidewater glaciers, where calving processes dominate mass loss and are estimated to account for up to 70% of the ice sheet's sea-level contribution by the end of the century (Goelzer et al., 2020; Choi et al., 2021). The fidelity of ice-sheet models in capturing such ice-ocean processes is often tested, and refined, against the satellite observation record. This implies that tidewater glacier behaviour can only be constrained across the most recent decades, when climatic conditions were distinctly cooler than what we expect in the future. Moreover, the ocean exhibits considerable natural variability on yearly to multi-decadal time scales. This complicates and potentially skews our interpretation of how oceanic changes affect the ice sheet (Khazendar et al., 2019). The geological record, however, can extend this history over centennial and millennial time scales to time periods similar to that of future projections. This provides valuable context for the observed ice-sheet behaviour over recent decades and important natural baselines and constraints for models of current and future ice-sheet change.

The Holocene interglacial period presents the opportunity to study Greenlandic glacier behaviour across three distinct phases: first, the recession of the GrIS during the deglaciation following the Last Glacial Maximum (LGM) in response to rapidly warming temperatures (11.7-8.2 ka BP); second, the response of the ice sheet to the Holocene Thermal Maximum (HTM, 8.2-4.2 ka BP), a protracted period when Arctic temperatures were $3\pm1°$C above pre-industrial averages (Briner et al., 2016; Kaufman and Broadman, 2023); and third, the neoglacial cooling that began as early as 6.5-6.3 ka BP (Davis et al., 2009) and led into the Little Ice Age (LIA) where margins of the GrIS re-advanced from a Holocene minimum towards a pre-industrial state (Kjær et al., 2022). Terrestrial studies have presented a detailed geological record of the GrIS margin evolution across different regions (e.g. Kelly and Bennike, 1992; England, 1999; Funder et al., 2011; Larsen et al., 2019; Young et al., 2021), culminating in a Greenland-wide reconstruction of ice-margin retreat during the early Holocene by Leger et al. (2023) (PaleoGrIS). Furthermore, marine geophysical mapping and marine sediment cores have provided additional knowledge of the timing of outlet glacier retreat and changing ice dynamics throughout the Holocene (Wangner et al., 2018; Reilly et al., 2019; Jakobsson et al., 2018; O'Regan et al., 2021). This is especially timely as paleo ice-sheet modelling efforts are using increasingly fine resolution (<3 km) in regional studies in order to accurately resolve fjord-scale glacier dynamics and to assess
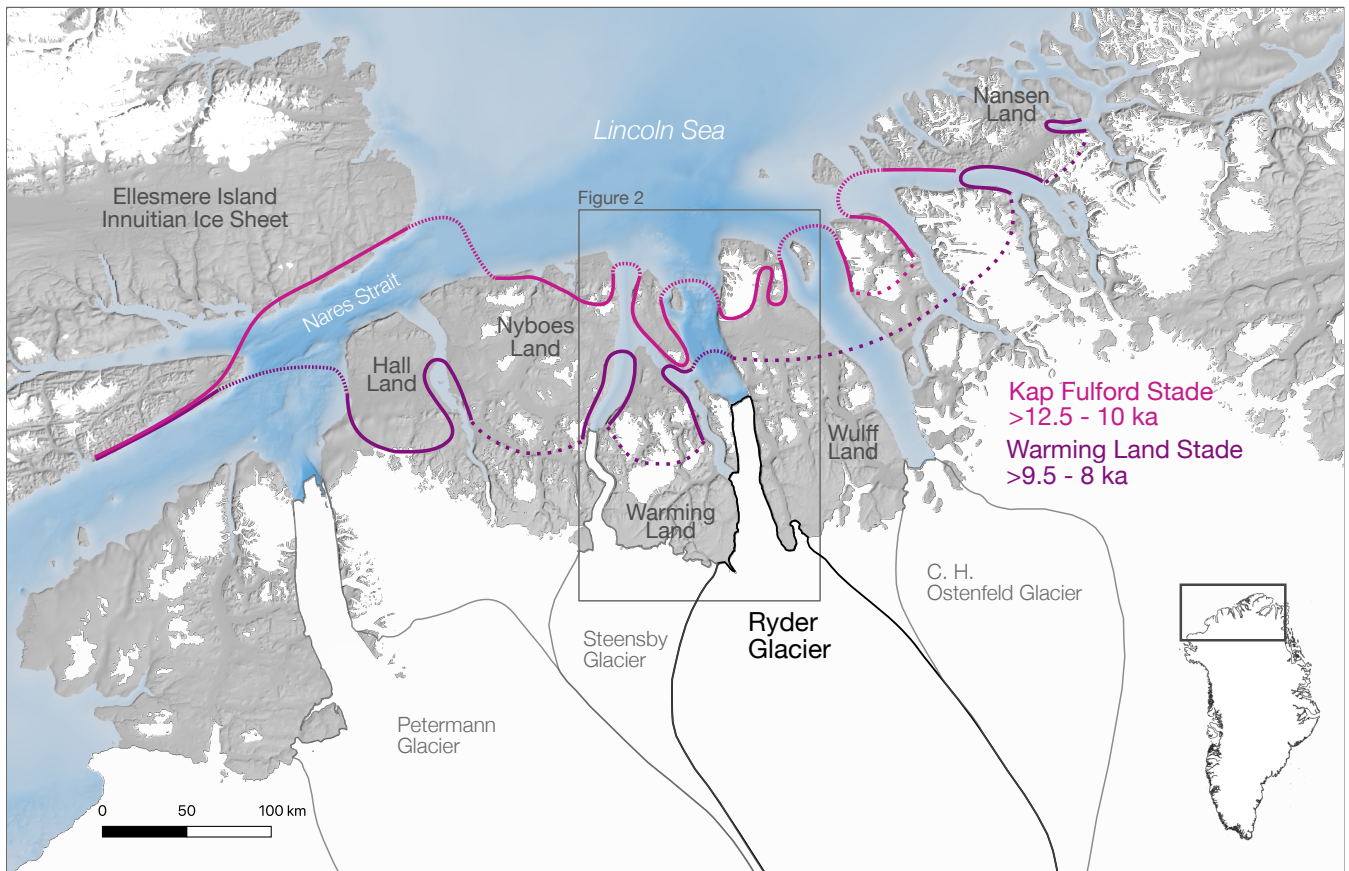
**Figure 1.** A map of Northern Greenland highlighting the contemporary drainage basins of Petermann, Steensby, Ryder and Ostenfeld Glaciers (Mouginot and Rignot, 2019). Paleo ice sheet margins of the Kap Fulford (>12.5 - 10 ka BP, pink) and Kap Warming Stade (>9.5 - 8 ka BP, purple) are shown as described in the terrestrial study by Kelly and Bennike (1992). Small dashed lines indicate hypothesised marine margins of GrIS, while large dashes are used to join data gaps.

the influence of ice-ocean interactions on the GrIS throughout the Holocene (Briner et al., 2020; Kajanto et al., 2020; Cuzzone et al., 2022).

55    Recognising the patterns and drivers of retreat during the Holocene, the current interglacial period, is especially pertinent to the Northern Sector of the GrIS. At the LGM, the ice sheet coalesced with the Innuitian Ice Sheet (England et al., 2006) and likely extended out into the Lincoln Sea where ice streams emanating from the Nares Strait and the northern fjords likely formed ice-shelf conditions (Dawes, 1986; England, 1999; Larsen et al., 2010). During the Holocene, this marine-based ice system collapsed, as the GrIS decoupled from the Innuitian Ice Sheet and the northern outlet glaciers retreated back into their
60    modern day fjords. Owing to the remote nature of the region and harsh sea-ice conditions, field surveys have been sparse and sporadic (Koch, 1928; Dawes, 1977; Weidick, 1978). Based on available data in the early 1990s, North Greenland's Holocene history was summarised into a series of "Stades" (Danish for stages) by Kelly and Bennike (1992) (Fig. 1). The Kap Fulford

Stade relates to the most recent ice-sheet maximum, the Late Weichselian Glaciation, when the northern glaciers extended to the outer fjords and the GrIS and Innuitian Ice Sheets remained coalesced in Nares Strait. The retreat from this last maximum ice-sheet extent is proposed to have occurred >10.5 cal ka BP by O'Regan et al. (2021), after combining new marine radiocarbon dates and existing terrestrial dates (Kelly and Bennike, 1992). The Warming Land Stade follows between >9.5 to 8 cal ka BP, corresponding to a well-developed moraine sequence that represents a standstill of glacial retreat 20 - 60 km inland of the Kap Fulford Stade. Finally, the Steensby Stade characterises the neo-glacial re-advance of the GrIS from its Holocene minimum towards its most recent maximum in the LIA. While the onset of this re-advance is poorly dated, it may have occurred prior to the late Holocene, perhaps as early as around 5.8 ka BP (O'Regan et al., 2021).

At present, Northern Greenland contains enough ice to raise global mean sea levels by ∼93 cm (Mouginot et al., 2019). However, mass loss had been relatively subdued from the region until the 2000s, likely due to the buttressing of inland ice provided by floating ice tongues limiting ice discharge (Hill et al., 2017; Millan et al., 2018, 2023). Since 1978, the region's ice tongues have lost ∼25% of their volume, with the notable collapse of Ostenfeld Glacier's ice tongue in 2003. Petermann, Steensby and Ryder Glaciers remain buttressed by their floating ice tongues, yet have all seen grounding-line retreat and an acceleration of ice discharge explicitly linked to increasing basal melt rates beneath the floating ice (Hill et al., 2018a; Millan et al., 2023). During the Holocene, the ice tongues of Petermann and Ryder Glacier are believed to have disintegrated and retreated inland of the current grounding-line positions (Jakobsson et al., 2018; Reilly et al., 2019; O'Regan et al., 2021). Such behaviour could serve as a potential analogy for the future evolution of the contemporary outlet glaciers, where the collapse of their floating ice tongues may accelerate ice discharge and the region's contribution to global sea-level rise (Hill et al., 2018b; Humbert et al., 2023).

Here we use the Ice-sheet and Sea-level System Model (ISSM; Larour et al., 2012) to explore the dynamics of Ryder Glacier during the Holocene, constrained by unique marine sediment archives, mapped submarine glacier landforms and terrestrial evidence. Focusing on a single outlet glacier allows us to employ a model that resolves ice-ocean and grounding line dynamics in high resolution (<1 km). This puts more confidence in our simulations and gives us the opportunity to provide a new, more detailed understanding of how Ryder Glacier and its ice tongue responded to a warming atmosphere and ocean.

## 2 Ryder Glacier

Ryder Glacier currently drains the GrIS into Sherard Obsorn Fjord (Fig 2), where a floating tongue extends ∼25 - 30 km from the grounding line and velocities peak at 500 m yr$^{-1}$ (Wilson et al., 2017; Hill et al., 2017). Sherard Osborn Fjord continues ∼70 km from the present day grounding line toward the Lincoln Sea, reaching a maximum depth of 890 m and containing two shallow bathymetric sills; an outer (375 - 475 m below sea level) and inner sill (193 - 390 m below sea level), with the latter thought to play a key role in shielding the glacier from sub-surface warm Atlantic Waters (AW) (Jakobsson et al., 2020; Nilsson et al., 2023). The floating terminus has remained relatively stable since the 1990s, undergoing a cyclic pattern of slow advance followed by retreat, potentially controlled by fjord geometry (Holmes et al., 2021). This stability has persisted despite a retreat of the grounding line by ∼8 km since 1992 (Millan et al., 2023).
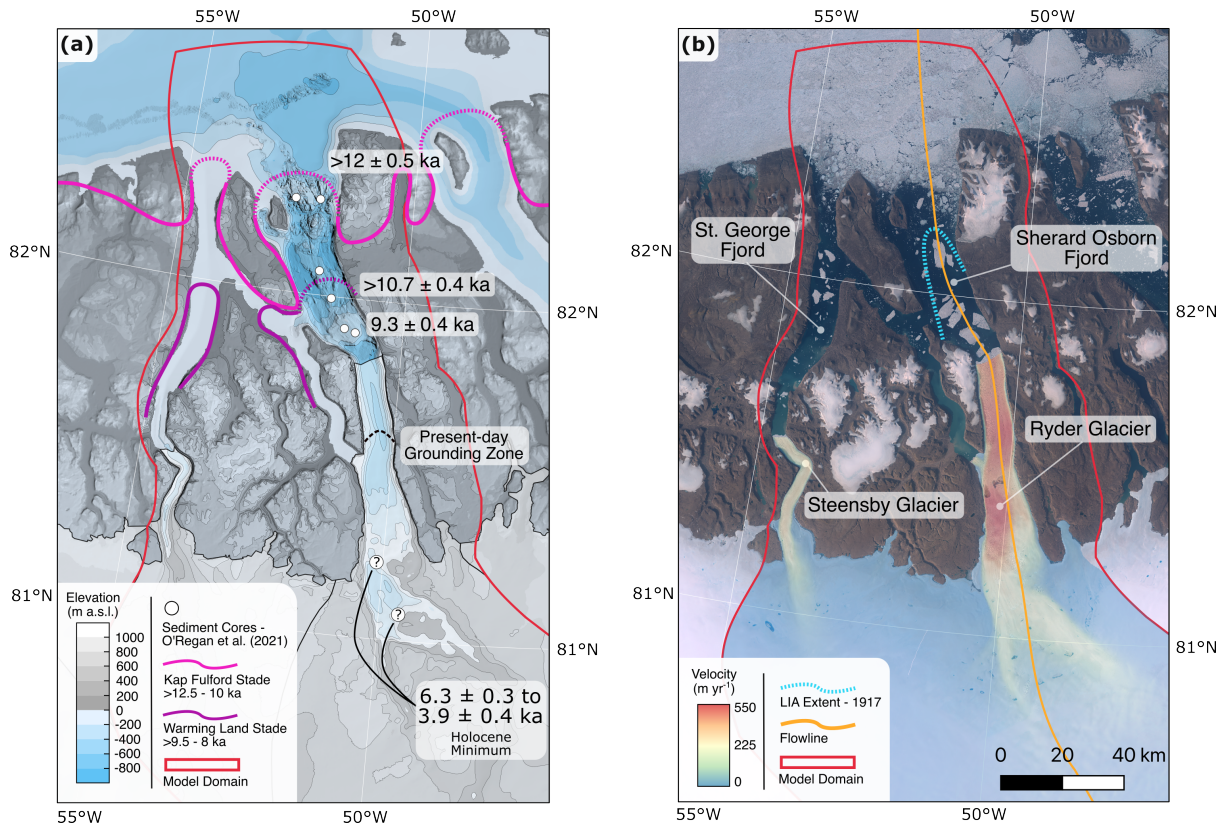
**Figure 2. (a)** A topographic map of Ryder and Steensby Glacier. Both the bathymetry and topography are taken from BedMachine v5 (Morlighem et al., 2022). Paleo ice-sheet margins of the Kap Fulford Stade (>12.5 - 10 ka BP, pink) and Warming Stade (>9.5 - 8 ka BP, purple) are redrawn from Kelly and Bennike (1992). Sediment cores taken during the Ryder Expedition on Icebreaker *Oden* are shown by white circles and are accompanied by minimum ages (O'Regan et al., 2021). **(b)** A satellite image of Ryder and Steensby glacier draining into Sherard Osborn and St. George Fjord from summer 2019 (MacGregor et al., 2020). Ice velocities are taken from MEaSUREs (Joughin et al., 2016; Joughin et al., 2018). A centre flowline for Ryder Glacier is shown in orange, the Little Ice Age extent of the glacier is highlighted in dashed blue (Koch, 1928) and the model domain used in the study is shown in red.

During the Ryder 2019 expedition with the Swedish Ice Breaker *Oden*, numerous sediment cores were taken in Sherard Osborn and have been used to describe the Holocene behaviour of Ryder Glacier by O'Regan et al. (2021) (Fig 2a). Radiocarbon dating and analysis of six lithologic units (LU) detail an evolution of the glacier that generally aligns with the terrestrial record of retreat described in Kelly and Bennike (1992). The first two lithologic units (LU6 and LU5) comprise a transition from glaciomarine diamicton to a laminated meltwater-dominated facies as the grounding line of Ryder Glacier began to retreat from the fjords' outer sill. Ages of $12 \pm 0.5$ ka BP (LU6) on the outer sill and $10.7 \pm 0.4$ ka BP (LU5) in the mid-fjord region align with the Kap Fulford Stade, while the beginning of sedimentation on the inner sill at $9.3 \pm 0.4$ ka BP (LU5) corresponds to the Warming Land Stade. A further laminated sub-ice shelf facies follows (LU4: $7.6 \pm 0.4$ to $6.3 \pm 0.3$ ka BP) before a

second diamict facies spanning $6.3 \pm 0.3$ to $3.9 \pm 0.4$ ka BP (LU3) occurs and hints at the collapse of the ice tongue during the HTM. The low sedimentation rates during this period are suggested to mark the retreat of Ryder Glacier into a small isolated embayment, $\sim 40$ km upstream of the present-day grounding line (Fig 2a). Such retreat would have reduced the delivery of fine-grained meltwater-entrained sediments but still allowed for icebergs to deposit IRD in the fjord. The following lithologic facies after $3.9 \pm 0.4$ ka BP (LU2 and LU1), inline with the Steensby Stade described by Kelly and Bennike (1992), show a transition from open-water bioturbated sediments to laminated facies that indicate the regrowth and advance of Ryder's ice tongue towards the outer sill. Lauge Koch mapped Ryder's LIA extent in 1917 during the Second Thule Expedition, showing the ice tongue had extended toward the mouth of Sherard Osborn Fjord and the outer sill (Fig. 2b).

## 3 Methods

The finite-element thermomechanical ice-sheet model ISSM is employed to simulate the Holocene history of Ryder Glacier (Larour et al., 2012) together with a Higher-Order (HO) approximation (Blatter, 1995; Pattyn, 2003) of the Full Stokes (FS) equations. We use the HO approximation as it balances computational efficiency with thermomechanical 3D ice dynamics, including higher-order stresses and temperature-dependent viscosity, which are critical when simulating ice evolution over paleo-timescales. Although we recognise that FS offers greater accuracy in regions such as the grounding line, where the inclusion of bridging stresses, neglected in the HO approximation, are important, it remains computationally infeasible to use over extended timescales such as the Holocene. To better capture grounding migration, we run our HO model at resolutions of < 1km, following a model setup that is similar to Briner et al. (2020) and Cuzzone et al. (2022) that performed well when simulating terrestrial and marine regions of the GrIS over the Holocene.

### 3.1 Model domain and set-up

Our model domain is based on the present-day drainage catchment of Ryder Glacier, defined from velocity and slope angles of the ice surface (Mouginot and Rignot, 2019). The domain is then extended northward to include Sherard Osborn Fjord and $\sim 30$ km north into the Lincoln Sea to capture the LGM extent of Ryder Glacier (Fig. 2b). On the eastern side of the domain we follow the topographic divide in Wulff Land, while also extending the domain westward to include the neighbouring Steensby Glacier and St. George Fjord. We do this in order to capture any effects arising from the two glaciers merging towards the Lincoln Sea owing to the connected fjord systems. We define the base of our domain using bedrock topography from BedMachine v5 (Morlighem et al., 2022), which contains the high-resolution bathymetric data of Sherard Osborn Fjord surveyed by Swedish Ice Breaker *Oden* in 2019 (Fig. 2a; Jakobsson et al., 2020). The initial ice surface for our model is also taken from Bedmachine v5, before it evolves in our Younger Dryas spin-up (Section 3.5).

A non-uniform mesh of the domain is produced from modern ice velocities and bedrock topography (Joughin et al., 2016; Morlighem et al., 2022). Elements range from 10 km in size for the slow-moving ice in the upper regions of the domain, decreasing to 750 m where velocities exceed 400 m yr$^{-1}$ as well as in contemporary ice-free fjord areas. This ensures that grounding-line migration is simulated at resolutions of <1 km for the entirety of our simulations, a resolution necessary for

capturing such dynamics (Seroussi and Morlighem, 2018). The domain is then extruded vertically to contain five layers, following Cuzzone et al. (2018) we use cubic finite elements along the z-axis (prisms P1×P3) for vertical interpolation to capture sharp thermal gradients near the base of the ice sheet without additional, computationally expensive, layers.

We use an enthalpy formulation from Aschwanden et al. (2012) to simulate ice temperature throughout our simulations, applying a constant geothermal heat flux at the base (Shapiro and Ritzwoller, 2004), and transient air temperatures at the surface (Section 3.4). The ice rheology parameter $B$ is initialised by solving for a present-day thermal state and allowed to vary transiently following the rate factors in Cuffey and Paterson (2010).

Basal friction is modelled through the linear viscous Budd Law (Budd et al., 1979), defining basal drag ($\tau_b$) as:

$$\tau_b = -k^2 N v_b \tag{1}$$

where $k$ is a friction coefficient, $N$ is effective pressure and $v_b$ is the basal velocity. The friction coefficient, $k$, for present day ice areas is inverted for using an adjoint method (Morlighem et al., 2010, 2013) that fits with modern velocities (Joughin et al., 2016; Joughin et al., 2018). For contemporary non-ice areas we define a friction coefficient as a function of elevation similar to Åkesson et al. (2018a):

$$k = 100 \times \frac{\min\left(\max(0, z_b + |\min(z_b)|, \max(z_b))\right)}{\max(z_b)} \tag{2}$$

where $z_b$ is the bedrock elevation relative to sea level (Morlighem et al., 2022). This produces a low friction coefficient in the deep fjords, where we would expect fast-flowing ice, and larger values across topographic highs, where ice is expected to flow slower. This spatial distribution of friction coefficients are kept fixed over time. Meanwhile, we follow Cuzzone et al. (2019) to allow the friction field to be scaled transiently based on changes in the simulated evolution of basal temperatures relative to basal temperatures from a present-day thermal steady state of the glacier. This implementation produces an increase in friction for colder temperatures during the YD, while also rendering more slippery conditions during warmer periods such as the HTM.

We apply Dirichlet boundary conditions of ice thickness, velocity and temperature on the eastern and western boundaries of our domain. These boundary conditions are taken from a continental scale model of GrIS simulated across the same timescales with a similar model setup, albeit at a coarser resolution (Briner et al., 2020). We use different boundary conditions for each of our SMB scenarios (Section 3.4), aligning with the experiments found in Briner et al. (2020). We justify the use of these boundary conditions as running a continental scale simulation at an equivalent resolution would be computationally infeasible. Furthermore, by using consistent boundary conditions across our model runs, we isolate the effects of our applied climate forcings on glacier behaviour. Finally, ice is allowed to freely leave the domain at the northern boundary.

All model simulations are run for 12,550 years from 12,500 BP, where P is defined as 1950 CE, to 2000 CE, using an adaptive time step that varies between 0.02 and 0.3 years while satisfying the Courant-Friedrichs-Lewy criterion (Courant et al., 1928).

## 3.2 Calving parameterisation and ice-front migration

Ice-front migration is handled within ISSM using the level-set method (Bondzio et al., 2016). The ice front boundary moves at velocity:

$$\mathbf{v}_f = \mathbf{v} - (c + M)\mathbf{n}, \tag{3}$$

where $\mathbf{v}$ is the velocity vector at the ice front, $c$ and $M$ are the calving and melting rate, respectively, and $\mathbf{n}$ is the normal vector pointing outward, orthogonal to the level-set defined as a signed-distance field. During our simulations we assume that horizontal melt at the front of an ice tongue is negligible compared to calving and ocean-induced melt from below. Thus, we focus on applying melt rates to beneath ice that has reached flotation (Section 3.3).

A von Mises law is used to parameterise calving (Morlighem et al., 2016), where the calving rate, $c$, depends on the von Mises tensile stress, $\widetilde{\sigma}$ and a predefined maximum stress threshold value, $\sigma_{\mathrm{max}}$ (Table 1), :

$$c = |\mathbf{v}| \frac{\widetilde{\sigma}}{\sigma_{\mathrm{max}}}. \tag{4}$$

As such, calving can only occur when $\widetilde{\sigma} > \sigma_{\mathrm{max}}$; when $\widetilde{\sigma} < \sigma_{\mathrm{max}}$ then $c = 0$. This calving parameterisation has been successfully used to simulate the migration of grounded and floating Greenlandic ice fronts in both modern (Morlighem et al., 2016; Choi et al., 2018; Åkesson et al., 2022), and paleo settings (Kajanto et al., 2020; Cuzzone et al., 2022).

## 3.3 Ocean melt

An ocean melt rate is applied to floating ice as a linear function of depth. Melt rate increases from 0 m yr$^{-1}$ at depths shallower than 100 m to a predefined *deepmelt* value at depths below 400 m (Table 1). This implementation matches the distribution of submarine melt found through both observations and ocean modelling of Ryder Glacier (Wilson et al., 2017; Wiskandt et al., 2023), capturing the highest melt rates towards the grounding line, driven by the interplay with subglacial discharges and warmer ocean waters, before decreasing in the cooler polar surface waters found in the upper hundred meters of the fjord. Horizontal melt at the front of the ice tongue is assumed negligible, in line with melt at depths shallower than 100 m and under the premise that frontal ablation is dominated by calving processes while submarine melt primarily acts near the grounding line beneath ice tongues (Wilson et al., 2017; Holmes et al., 2021). In the event of an ice-tongue collapse, melt is applied uniformly to the submerged grounded glacier front at half the defined *deepmelt* value in order to account for a decrease in melt towards the water line.

## 3.4 Holocene climate

Holocene SMB is computed using a Positive Degree Day (PDD) model (Tarasov and Peltier, 1999), forced with paleoclimate reanalysis data from Badgeley et al. (2020). The model assumes that snow melts at 3 mm ºC$^{-1}$d$^{-1}$ followed by ice melt at 8
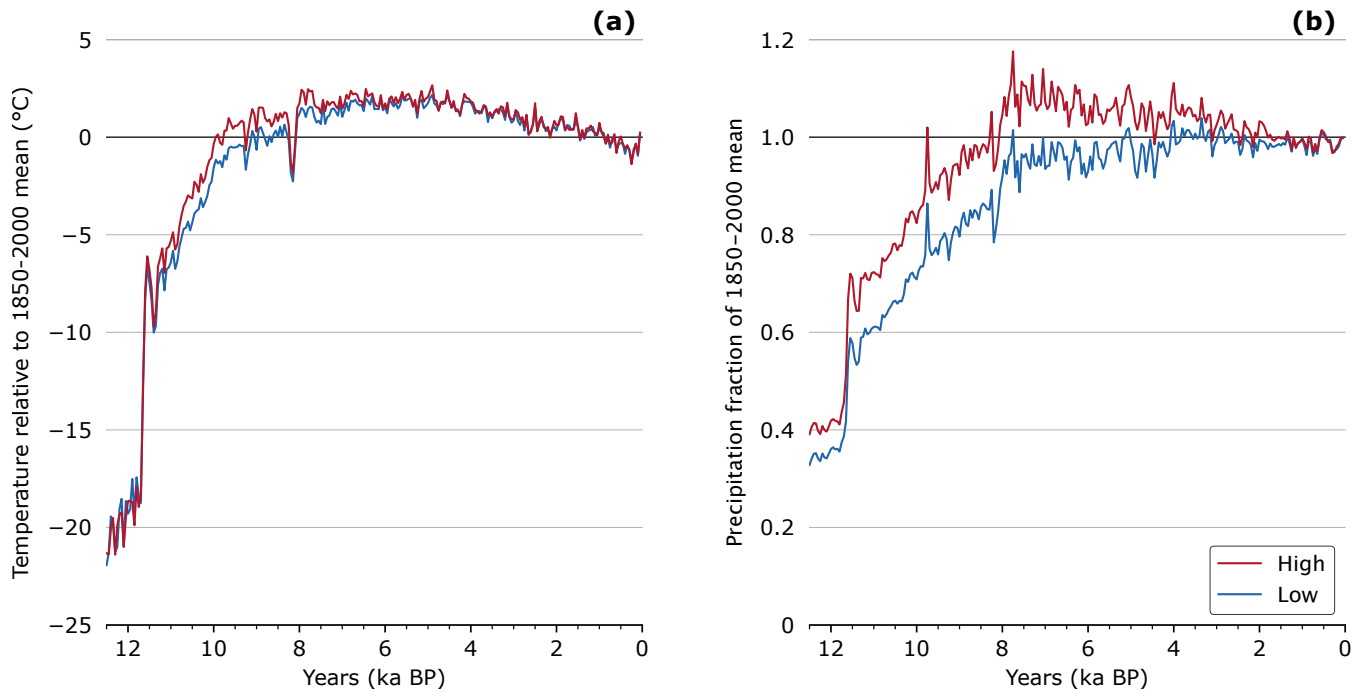
**Figure 3.** Mean annual climate data during the Holocene averaged over the model domain taken from Badgeley et al. (2020). **(a)** High (red) and low (blue) Holocene temperature scenarios expressed as anomalies with respect to a 1850 to 2000 mean (Box, 2013). **(b)** High (red) and low (blue) Holocene precipitation scenarios expressed as fractions of a 1850 to 2000 mean (Box, 2013).

mm ℃$^{-1}$d$^{-1}$ for the remaining positive degree days (Braithwaite, 1995; Born and Nisancioglu, 2012; Plach et al., 2018). The formation of superimposed ice is allowed following Janssens and Huybrechts (2000). Finally, a lapse rate of 6°C km$^{-1}$ is used
195    to adjust the climate forcings to transient changes in the glacier's elevation.

Temperature and precipitation for the PDD model is taken from a paleoclimate reanalysis dataset produced by Badgeley et al. (2020) through the assimilation of climate model simulations and proxy data. The TraCE21Ka climate model output (Liu et al., 2009; He et al., 2013) is used in conjunction with oxygen-isotope records from eight ice cores and ice-layer thicknesses from five ice cores to reconstruct temperature and precipitation, respectively. The resulting dataset contains a number of different
200    temperature and precipitation pathways, varying spatially at a 50-year temporal resolution, covering the Holocene.

We follow Cuzzone et al. (2022) in using four different Holocene SMB forcings produced from combinations of the high and low reconstructions of temperature and precipitation (Fig. 3a and b). These reconstructed variables represent the upper and lower bands of scenarios discussed in Badgeley et al. (2020) and provide a cost effective way of testing the impact of both climate drivers during the Holocene. We hereby refer to each SMB scenario using the following notation: Tempera-
205    ture/Precipitation; where, for example, High/Low would describe the SMB scenario produced from the high-temperature and low-precipitation pathways.
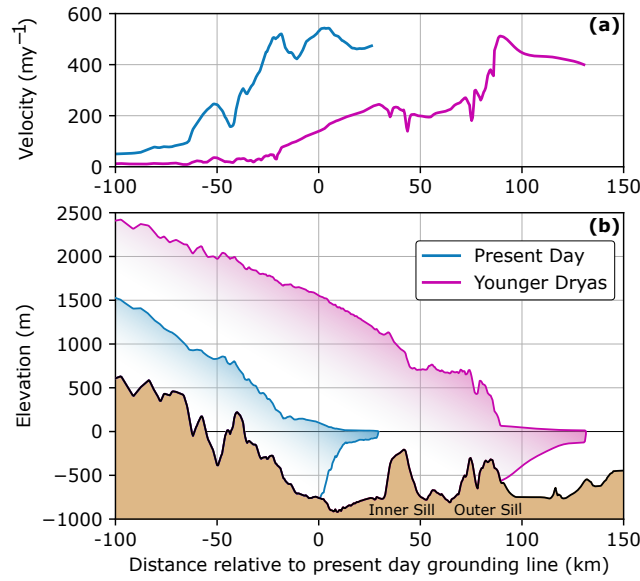
**Figure 4.** A comparison between the present day Ryder Glacier (blue) and that of the glacier after running a 20,000 year spin-up forced with a YD climate from SMB scenario Low/High (pink). **(a)** The velocity profile along the glacier's centre flowline. **(b)** A 2D cross section profile along the centre flowline. Bedrock data and the present day ice surface is from BedMachine v5 (Morlighem et al., 2022). Spin-up geometry from all SMB scenarios can be found in Fig. A2.

The aforementioned paleoclimate variables, temperature and precipitation, are expressed as anomalies from an 1850-2000 mean and a fraction of an 1850-2000 mean respectively. We therefore use the comparable monthly climate variables from Box (2013) to produce the final temperature and precipitation variables need for the PDD model:

$$T_t = \overline{T}_{1850-2000} + \Delta T_t, \tag{5}$$

$$P_t = \overline{P}_{1850-2000} \times \Delta P_t, \tag{6}$$

where $\overline{T}_{1850-2000}$ and $\overline{P}_{1850-2000}$ are monthly mean temperature and precipitation date from Box (2013), and $\Delta T_t$ and $\Delta P_t$ are the corresponding paleo anomalies from Badgeley et al. (2020). Every model run uses the Holocene climatology from 12,500 BP until 1850 CE, with the final 150 years using the mean modern values from Box (2013).

### 3.5 Younger Dryas spin-up

We perform a Younger Dryas (YD) model spin-up to obtain an initial ice-sheet state that is both geologically consistent and internally coherent. We assume that Ryder Glacier remained stable during the YD, consistent with the earliest recovered sediments from Sherard Osborn Fjord ($12 \pm 0.5$ ka BP), which indicate that the grounding line had not yet begun to retreat and

was likely positioned on the outer sill (O'Regan et al., 2021). Although other sectors of the Greenland Ice Sheet (GrIS) began to retreat from their LGM extents prior to the YD, retreat in the northern sector was comparatively limited (Leger et al., 2023). In this region, the grounding lines of the major outlet glaciers remained stable at or near the fjord mouths, typically grounded on bathymetric highs, until the onset of early Holocene warming (Kelly and Bennike, 1992; England, 1999; Jennings et al., 2011; Jakobsson et al., 2018; Jennings et al., 2019; O'Regan et al., 2021).

We begin our spin-up simulations using an initial modern-day ice surface from BedMachine v5 (Morlighem et al., 2022) and force the model with a constant climate from 12,500 BP. We conduct a spin-up for the four different SMB scenarios, maintaining consistent boundary conditions of ice thickness, temperature and velocities from the larger continental-scale model (cf. Section 3.1). It takes 20,000 model years until ice volume, temperature, and velocities reach an equilibrium. We do not allow calving during the spin-up. Ocean melt is applied after the first 2,000 years, in order to allow for grounding line advance, after which the *deepmelt* rate is set to 10 m yr$^{-1}$. While an arbitrary choice, we argue that ocean melt at the YD would be substantially lower than contemporary rates at Ryder Glacier (Wilson et al., 2017), due to both colder ocean temperatures and a reduction in subglacial discharge in a climate with little surface melt (Fig. 3a). The combination of ocean melt and atmospheric forcings results in a spun-up Ryder Glacier that aligns with the geological record at the YD, with the grounding line resting atop the outer sill where the oldest sediments recovered from Sherard Osborn Fjord are dated to $12 \pm 0.5$ ka BP (Fig. 4; O'Regan et al., 2021). Furthermore, the ice shelf emanating from the fjord also matches the hypothesised Lincoln Sea Ice Stream and ice shelf conditions across Northern Greenland (Funder and Larsen, 1982; Dawes, 1986; Larsen et al., 2010). The final spun-up state across the four different SMB scenarios is very consistent (Fig. A2), owing to little climatic variation between the SMB scenarios at the YD (Fig. 3). These four YD states provide the initial conditions for our Holocene transient runs.

## 3.6 Transient experiments

Our transient experiments are designed to assess how atmospheric and ocean-ice interactions influenced the retreat of Ryder Glacier in the Holocene. We begin with five initial oceanic scenarios that vary the calving threshold (Section 3.2), and ocean *deepmelt* rate (Section 3.3), from modern *Reference* values (Table 1). These five sets of ocean forcings are run across the four different Holocene SMB scenarios previously discussed (Section 3.4).

Our *Reference* calving threshold for floating ice is 300 kPa as this value was able to reproduce the recent evolution of Ryder Glacier's floating tongue (Fig. A1) and aligns with the threshold used in a study of the neighbouring Petermann glacier by Åkesson et al. (2022). Because calving laws are often calibrated for glaciers in specific states, influenced by factors such as fjord geometry, bedrock topography, and ice rheology (Amaral et al., 2020; Wilner et al., 2023), we acknowledge that our chosen *Reference* calving threshold is unlikely to remain valid throughout the entire Holocene. To evaluate the influence of the calving threshold on ice dynamics, we conduct transient simulations with varied threshold values. For our *High_Calving* scenario, we lower the threshold to be 200 kPa to implicitly account for an extended calving period during the HTM when sea ice conditions were more seasonal (Detlef et al., 2023). Conversely, we set a threshold of 1000 kPa for our *Low_Calving* scenario, the same value as our grounded ice calving threshold, with the idea of preserving Ryder Glacier's floating tongue throughout the Holocene. At the beginning of all transient runs the floating calving threshold is set to 1000 kPa before linearly

**Table 1.** A summary of different ocean forcings with respective calving thresholds for floating ice and submarine melt values. In bold are the ocean scenarios that are only run with the upper and lower SMB scenarios (Fig.3); high-temperature and low-temperature (High/Low) as well as low-temperature and high-precipitation (Low/High). Note that the spin-up stimulations do not include calving.

| Ocean Scenario | *Deepmelt* (m yr$^{-1}$) | Calving Threshold (kPa) |
|---|---|---|
| Spin-up | 10 | - |
| Reference | 40 | 300 |
| Low Melt | 10 | 300 |
| High Melt | 100 | 300 |
| Low Calving | 40 | 1000 |
| High Calving | 40 | 200 |
| **Low** | 10 | 1000 |
| **High** | 100 | 200 |

transitioning to the defined value in the ocean scenario between 11,500 ka BP and 10,000 ka BP as temperatures rise from the YD into the Holocene.

255    For melt under the floating tongue, we set our *Reference* value for *deepmelt* to be 40 m yr$^{-1}$. This aligns with oceanic modelling studies of Ryder Glacier, as well as satellite observations of Ryder and other northern Greenlandic glaciers (Wilson et al., 2017; Millan et al., 2023; Wiskandt et al., 2023). For a *High_Melt* scenario we set the *deepmelt* rate as 100 m yr$^{-1}$, similar to modelled peak melt rates under Ryder Glacier's ice shelf with a warming of AW temperatures by 2°C (Wiskandt et al., 2023). For a *Low_Melt* scenario we take a *deepmelt* rate of 10 m yr$^{-1}$, the same value used in the YD model spin-up.

260    The transition from a consistent *deepmelt* rate of 10 m yr$^{-1}$ during our spin-up simulations to the defined melt rate for the transient simulation occurs linearly between 11,500 BP and 10,000 BP.

Furthermore, we run two extreme ocean scenarios, here termed *High* and *Low*, where we combine the respective *deepmelt* rates and floating calving thresholds from their individual high and low scenarios together. These two ocean scenarios are only run with the upper and lower limits of our SMB pathways.

265    **4   Results**

Here we describe the results of our Holocene transient simulations of Ryder Glacier by first focusing on the marine retreat and ice dynamics of the glacier (Section 4.1), followed by the terrestrial evolution of the ice-sheet margin (Section 4.2).
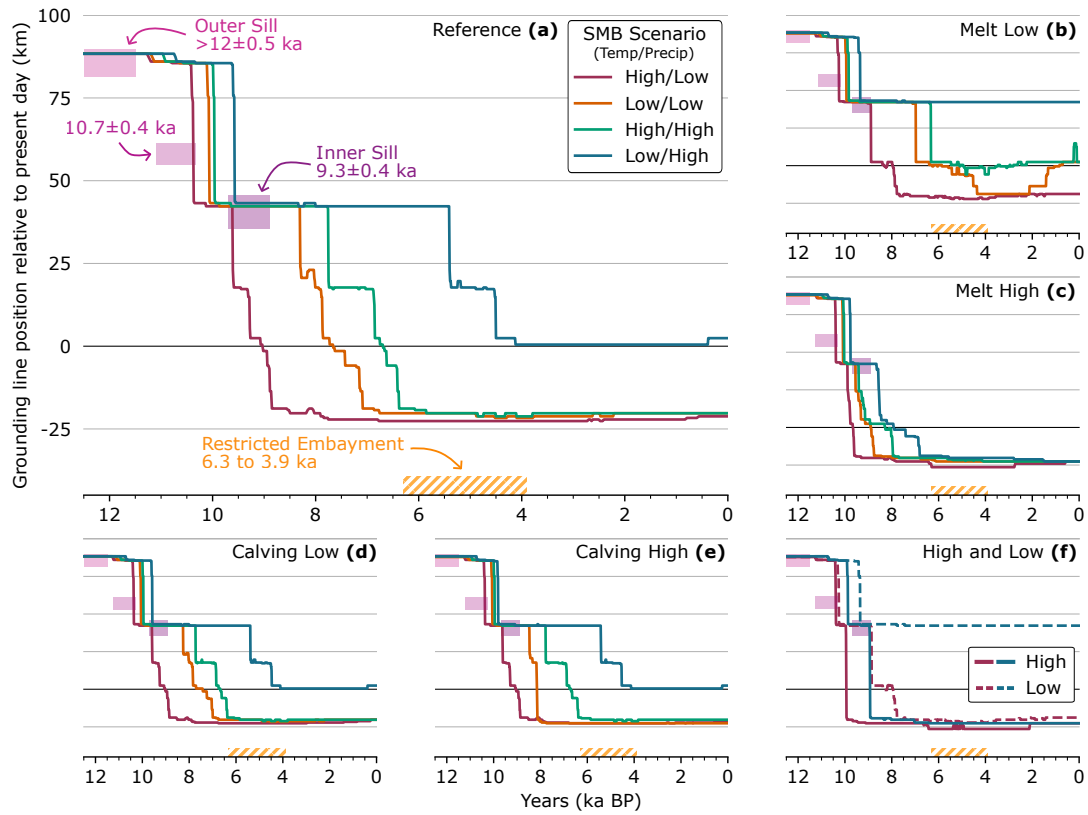
**Figure 5.** Evolution of the grounding line relative to Ryder's present day position for all transient runs. Line colour defines the SMB scenario for the transient runs: High/Low (red), Low/Low (Orange), High/High (Green) and Low/High (Blue). Each subplot represents a different ocean scenario: **(a)** *Reference*, **(b)** *Melt_Low*, **(c)** *Melt_High*, **(d)** *Calving_Low*, **(e)** *Calving_High* and **(f)** both the extreme *High* and *Low* ocean forcings. Shaded boxes highlight the position of sediment cores and their minimum ages, alongside possible timing of retreat into the restricted embayment upstream of the present day grounding line. All dates are sourced from O'Regan et al. (2021).

## 4.1 Marine Holocene evolution

The evolution of Ryder Glacier in our simulations is described in the context of the lithologic units (LU) taken from sediment
270 cores taken in Sherard Osborn Fjord that can be used for an idealised comparison of the glacier's behaviour (O'Regan et al., 2021).

### 4.1.1 Early Holocene retreat

Ryder Glacier retreats from the outer sill between 10.4 and 9.4 ka BP in all of our Holocene simulations (Fig. 5). This is ∼2000 years later than indicated by the age of the oldest sediments recovered from the outer sill in Sherard Osborn Fjord, which are
275 dated to $12 \pm 0.5$ ka BP (LU6). The simulated retreat dates instead align well with the basal age of the next lithologic boundary,
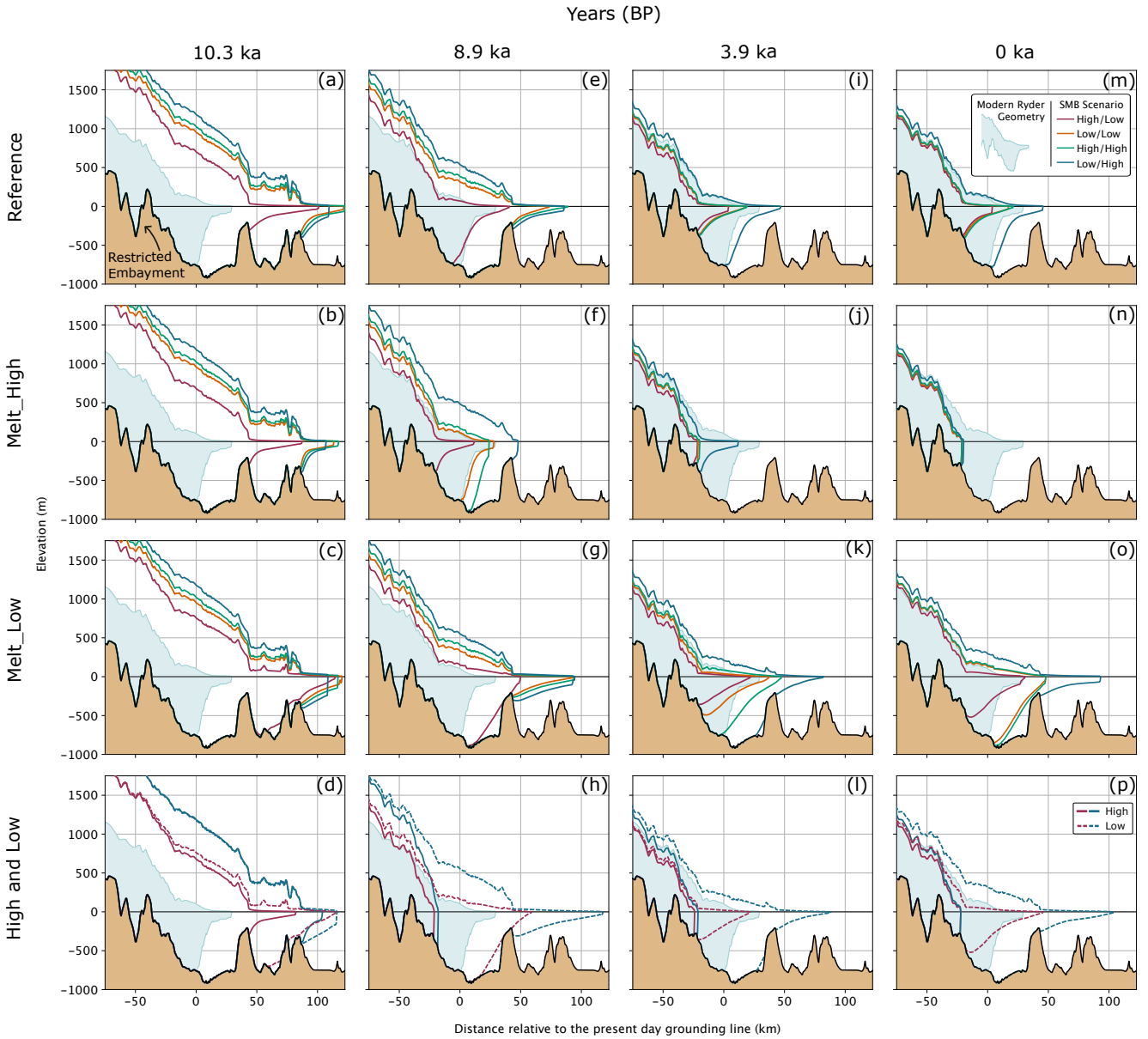
**Figure 6.** Evolution of Ryder Glacier in 2D cross section views along the centre flowline during the Holocene at specific time stamps. Dates of 10.3 ka **(a-d)**, 8.9 ka **(e-h)**, 3.9 ka **(i-l)** and 0 ka **(m-p)**, represent specific landmarks in the evolution of Ryder as discussed in O'Regan et al. (2021). Each row represents a different ocean forcing used in the transient simulation (Table 1), from top down this includes: *Reference*, *Melt_High*, *Melt_Low* and both extreme *High* and *Low* Scenarios. Ocean scenarios *Calving_High* and *Calving_Low* are found in the supplementary information as their behaviour does not differ considerably from the *Reference* scenario (Fig. A3). Each plot contains the 4 different SMB scenarios: High/Low (red), Low/Low (Orange), High/High (Green) and Low/High (Blue).

LU5, dated to $10.7 \pm 0.4$ ka BP, found between both sills in Sherard Osborn Fjord which marks the beginning of sedimentation in the mid-fjord region (Fig. 2a).

There is minimal variation in the timing of retreat from the outer sill across the different ocean scenarios (Fig. 5), with the glacier's geometry very consistent at 10.3 ka (the minimum age of LU5; Fig. 6 a-d). Instead, retreat varies with the choice of SMB pathways, that is, for high or low scenarios of temperature and precipitation. Simulations using the High/Low (temperature/precipitation) scenario retreat first (10.4 to 10.2 ka BP), followed by Low/Low (10.2 to 9.9 ka BP) and High/High (10 to 9.8 ka BP) and finally Low/High (9.8 to 9.4 ka BP). We consistently observe that this sequence of SMB scenarios dictates the timing of retreat within each ocean forcing throughout the Holocene (Fig. 5).

While the timing of retreat from the outer sill differs between SMB scenarios, the pattern and pace of retreat does not. In all runs, once Ryder begins to detach from the outer sill the grounding line quickly retreats $\sim$40 km in less than 50 years (Fig. 5), implying a mean retreat rate >800 m yr$^{-1}$. Notably, there is no grounding-line standstill in the deeper mid-fjord, and continuous retreat is observed, irrespective of the choice of atmospheric and oceanic forcing, until the grounding line reaches the inner sill. Here, the grounding line remains stable in all runs for at least 500 years. It is noted here that simulations Low/High: *Melt_Low* and Low/High: *Low* do not retreat further than the inner sill (Fig. 5 b and f).

Our simulations show a wide range of dates for retreat from the inner bathymetric high: 9.7 to 5.4 ka BP (Fig. 5). For runs forced with ocean scenarios: *Reference*, *Calving_Low* and *Calving_High*, retreat ages are consistently between 9.6 and 5.4 ka BP (Fig. 5a, d and e). The timing of retreat for simulations using the *Melt_Low* ocean forcing is later, between 8.9 and 6.4 ka BP, albeit with Low/High: *Melt_Low* remaining on the inner sill for the remainder of the Holocene simulation (Fig. 5b). Dates of retreat from the inner sill are earlier and much more concentrated for runs forced with *Melt_High* and *High* ocean scenarios, at 9.9 to 8.7 ka BP and 10 to 9 ka BP, respectively (Fig. 5 c and f).

It is only in simulations using an elevated ocean melt in *Melt_High* and *High* ocean forcing, as well as all runs forced with the most extreme SMB of high-temperature and low-precipitation (High/Low), that we see both grounding line retreat and the floating tongue detached from the inner sill that matches the onset of continuous sedimentation at this location: $9.3 \pm 0.4$ ka BP (LU5; Fig. 6e-h). All remaining simulations remain grounded on the inner sill until at least $\sim$8.3 ka BP (Fig 5).

### 4.1.2 Holocene minimum and ice tongue collapse

Ryder Glacier's Holocene minimum extent is captured by the sediment unit LU3 found throughout sediment cores taken in Sherard Osborn Fjord and spanning $6.3 \pm 0.3$ to $3.9 \pm 0.4$ ka BP. This unit marks a period of low sedimentation and the presence of IRD, interpreted by O'Regan et al. (2021) as the collapse of the ice tongue and the retreat of the glacier into the restricted embayment $\sim$40 km upstream of the contemporary grounding-line position (Fig. 2a).

None of our transient Holocene simulations match, in detail, this hypothesised retreat to the restricted embayment (Fig. 6). We simulate a maximum retreat of Ryder Glacier to just in front of the restricted embayment, $\sim$25 km behind the present day grounding-line position (Fig. 5). A retreat to this position occurs in all simulations using the *Reference* ocean forcing with the exception of the run using the mildest SMB scenario Low/High (Fig. 5a). Timing of retreat again follows the same pattern of
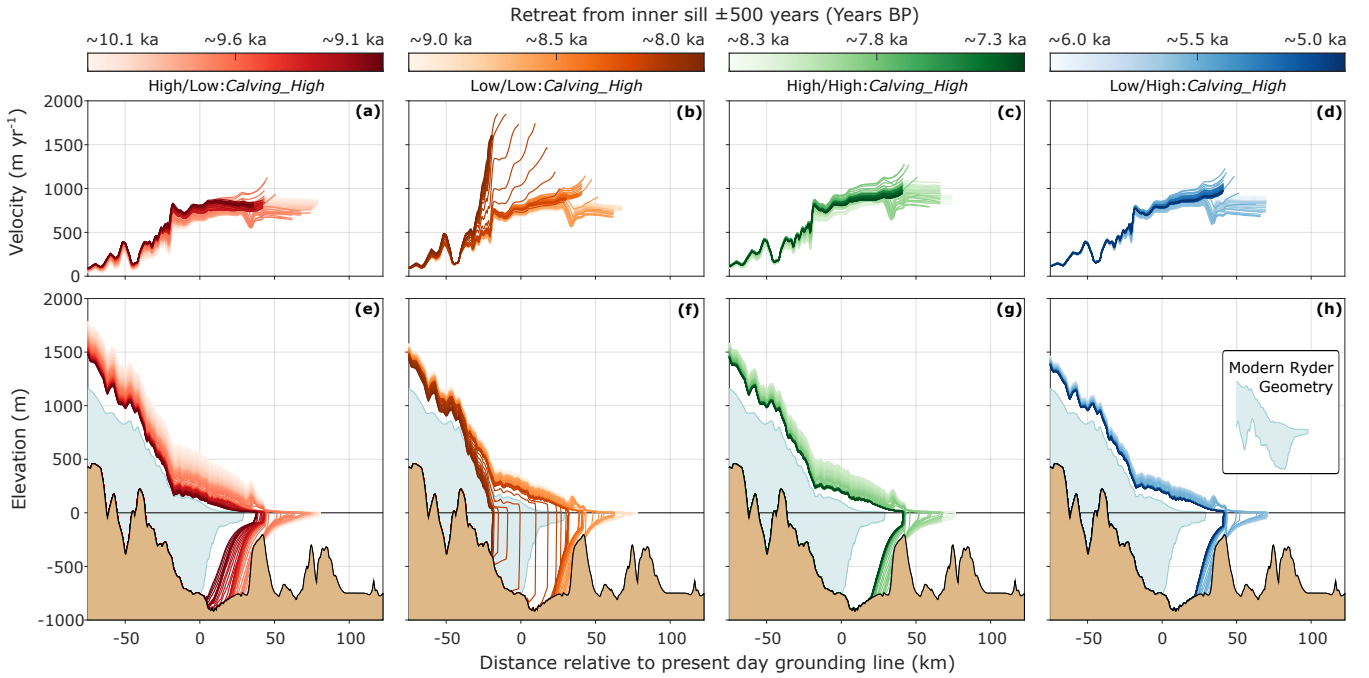
**Figure 7.** Ice dynamics of Ryder Glacier in the 500 years prior to and after retreat from the inner sill in Sherard Osborn Fjord for all transient runs forced with the *Calving_High* ocean scenario. (**a-d**) Changes in velocity along the centre flowline. (**e-h**) Changes in the geometry of Ryder Glacier using 2D cross sections from the centre flowline.

SMB; with a Holocene minimum occurring at 7.9 ka BP for SMB High/Low, 7.1 ka BP for Low/Low, 6.4 ka BP for High/High
310    ka BP and 4.5 ka BP for Low/High.

The same timing and extent of retreat are also found in the *Calving_High* and *Calving_Low* scenarios, with the exception of run Low/Low: *Calving_High* that retreats ∼900 years earlier (8 ka BP) than its *Reference* run due to the collapse of the floating tongue (Fig. 7). For *Melt_Low* simulations, a similar Holocene minimum position of ∼25 km behind the present-day grounding line is reached with High/Low and Low/Low SMB scenarios, albeit later than their *Reference* ocean simulations,
315    while High/High: *Melt_Low* does not retreat past the present-day grounding line (Fig. 5 a and b). All runs using the *Melt_High* ocean forcing retreat to this common Holocene minimum position, but again retreat is found to be both faster and more concentrated, with a minimum extent of Ryder reached between 9.5 and 6.5 ka BP.

We find Ryder's floating tongue collapses during our Holocene simulations in two distinct manners. The first occurs when Ryder retreats from the inner sill (c. at km 40 in Fig. 7). This happens in both runs using the *High* ocean forcing as well as
320    Low/Low: *Calving_High*. Figure 7 compares the retreat of all four *Calving_High* simulations for the 500 years before and after the grounding line detaches from the inner sill. Runs forced with SMB scenarios: High/Low, High/High and Low/High follow the same pattern of behaviour, albeit the timing of retreat differs. Therein, Ryder's retreat from the inner sill is followed by a steady grounding-line retreat of between 20 and 30 km in the following 500 years (Fig. 7 e, g and h). Terminus velocities prior to
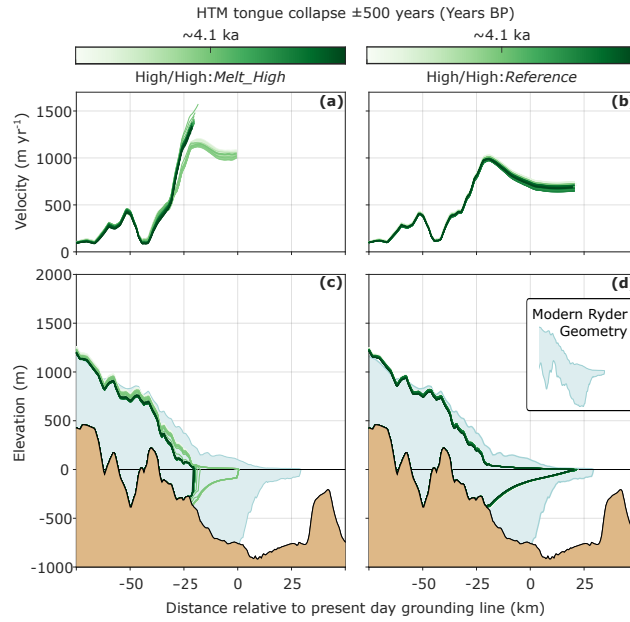
**Figure 8.** Ice dynamics in the 500 years prior to and after the loss of the floating tongue during the transient run High/High:*Melt_High* and ice dynamics of the High/High:*Reference* during the same period. (**a-b**) Change in velocity along the centre flowline. (**c-d**) Change in the geometry of Ryder Glacier using a 2D cross section from the centre flowline.

the retreat from the sill are $\sim 750$ m yr$^{-1}$, increasing to >1,000 m yr$^{-1}$ as the grounding line retreats from the bathymetric high, before gradually subsiding below 1,000 m yr$^{-1}$. Run Low/Low: *Calving_High* initially follows the same behaviour; however, large calving rates which remove the majority of the floating tongue coincide with an acceleration of terminus velocities to $\sim$1900 m yr$^{-1}$ and the glacier retreats as a sheer cliff face 35 km in $\sim$40 years (Fig. 7 b and f). The glacier then rests at its Holocene minimum as a grounded tidewater glacier, with terminus velocities of $\sim$1600 m yr$^{-1}$.

The second mechanism for tongue collapse occurs in all runs forced with the *Melt_High* ocean scenario. This behaviour is exemplified in Figure 8 by run High/High: *Melt_High* where the glacier, with the grounding line already at its Holocene minimum, sees its 25 km tongue disintegrate and terminus velocities accelerate from $\sim$1,000 m yr$^{-1}$ to $\sim$1,500 m yr$^{-1}$. No further grounding-line retreat is observed, as the glacier remains in shallow waters in front of the restricted embayment. The timing of collapse varies depending on SMB scenarios: High/Low at 7.5 ka BP, Low/Low at 6.2 ka BP, High/High at 4.1 ka BP and finally Low/High at 2.1 ka BP. The collapse behaviour is contrasted by the use of the *Reference* ocean forcing in High/High: *Reference* (Fig 8b and d), where a floating tongue of almost 50 km in length is sustained throughout the Holocene and velocities at the terminus remain consistently between 600 and 700 m yr$^{-1}$.

### 4.1.3 Neoglacial regrowth

The final lithologic units found in Sherard Osborn fjord, beginning at 3.9 ± 0.4 ka BP, are characterised by increased sedimentation rates and the deposition of laminated sediments, marking the advance of the grounding line and the eventual regrowth of
340 Ryder's ice tongue towards its LIA maximum (Fig. 2b).

In our transient simulations, we only find a late Holocene re-advance of the grounding line using the *Melt_Low* or extreme *Low* ocean forcing (Fig. 5b and f). Therein, the most pronounced readvance occurs in the Low/Low: *Melt_Low* run where the grounding line migrates ∼25 km. The re-advance is more subtle in runs High/Low: *Melt_Low* and High/High:*Melt_Low* at ∼10 km, although substantial thickening upstream of the grounding is observed (Fig. 6k and o). This same pattern of thickening is
345 observed in runs Low/High:*Melt_Low* and Low/High:*Low*, although the grounding line, which has not retreated from the inner sill during the HTM, does not show any advance. In all aforementioned runs, the floating tongue advances into Sherard Osborn Fjord at a similar rate to grounding line migration. In runs where the grounding line does not readvance, such as those using the *Reference* ocean scenario (Fig. 6i and m), there is no increase in length of the floating tongue towards the LIA maximum. Furthermore, there is no regrowth of the floating tongue in runs where a collapse occurs in the mid-Holocene (Fig. 6j and n).

350 ## 4.2 Terrestrial Holocene evolution

Here we explore the evolution of the terrestrial ice-sheet margin during our simulations in the context of reconstructed ice-sheet isochrones found in the PaleoGrIS database (Leger et al., 2023). Firstly, we assess the simulated retreat of the ice-sheet margin during the early Holocene from 10 ka to 8 ka BP (Section 4.2.1), over which time our model domain transitions from nearly entirely ice covered to roughly the same ice coverage as found at present-day (Fig. A4). 8 ka BP also marks a pause in ice
355 retreat found across all our simulations, likely relating to the Warming Land Stade inferred by Kelly and Bennike (1992) (Fig. A4). Furthermore, we describe the neoglacial advance of the ice-sheet margin by comparing a minimum ice extent, taken at 6 ka BP for all runs except those forced with SMB scenario Low/High when the minimum occurs later at 4 ka BP (Fig. A4), with the final state of our simulation representing present day (Section 4.2.2).

### 4.2.1 Warming Stade retreat

360 Retreat rates of the terrestrial ice margin vary considerably with the choice of SMB scenario (Fig. 9). The most negative SMB scenario, comprised of high-temperature and low-precipitation (High/Low), produces an ice margin that is consistently 30 - 40 km behind the reconstructed margin from the geological archive (Fig. 9a, e and i). The ice margins from simulations using the Low/Low (Fig. 9b, f and j) and High/High (Fig. 9c, g and k) SMB scenarios follow a similar retreat rate during the early Holocene, yet still exceed the rate of retreat from reconstructed isochrones across Warming Land despite more closely matching
365 the retreat around Steensby Glacier and St. George Fjord. Finally, simulations using the least negative SMB scenario, containing low-temperature and high-precipitation (Low/High), produce a retreat that tracks the reconstructed isochrone especially well at 9 and 8 ka BP, despite producing a slightly slower retreat at 10 ka BP (Fig. 9 d, h and l).

**Figure 9.** Evolution of the ice sheet margin in the model domain at 10 **(a-d)**, 9 **(e-h)** and 8 **(i-l)** ka BP. The various SMB scenarios are grouped into columns, while coloured ice sheet margins depict the ocean scenario used in each simulation: *Reference*: navy, *Melt_Low*: light blue, *Calving_Low*: blue, *Melt_High*: light orange and *Calving_High*: dark orange. Purple lines represent the reconstructed ice sheet margins from the PaleoGrIS database (Leger et al., 2023).

While the reconstructed ice margins from the PaleoGrIS database provide valuable insights into the Holocene extent of GrIS, we note that the isochrones across Northern Greenland are rated with *low* confidence, the third lowest of four confidence levels discussed in Leger et al. (2023). This is due to the sparse number of radiocarbon ages and the almost complete lack of
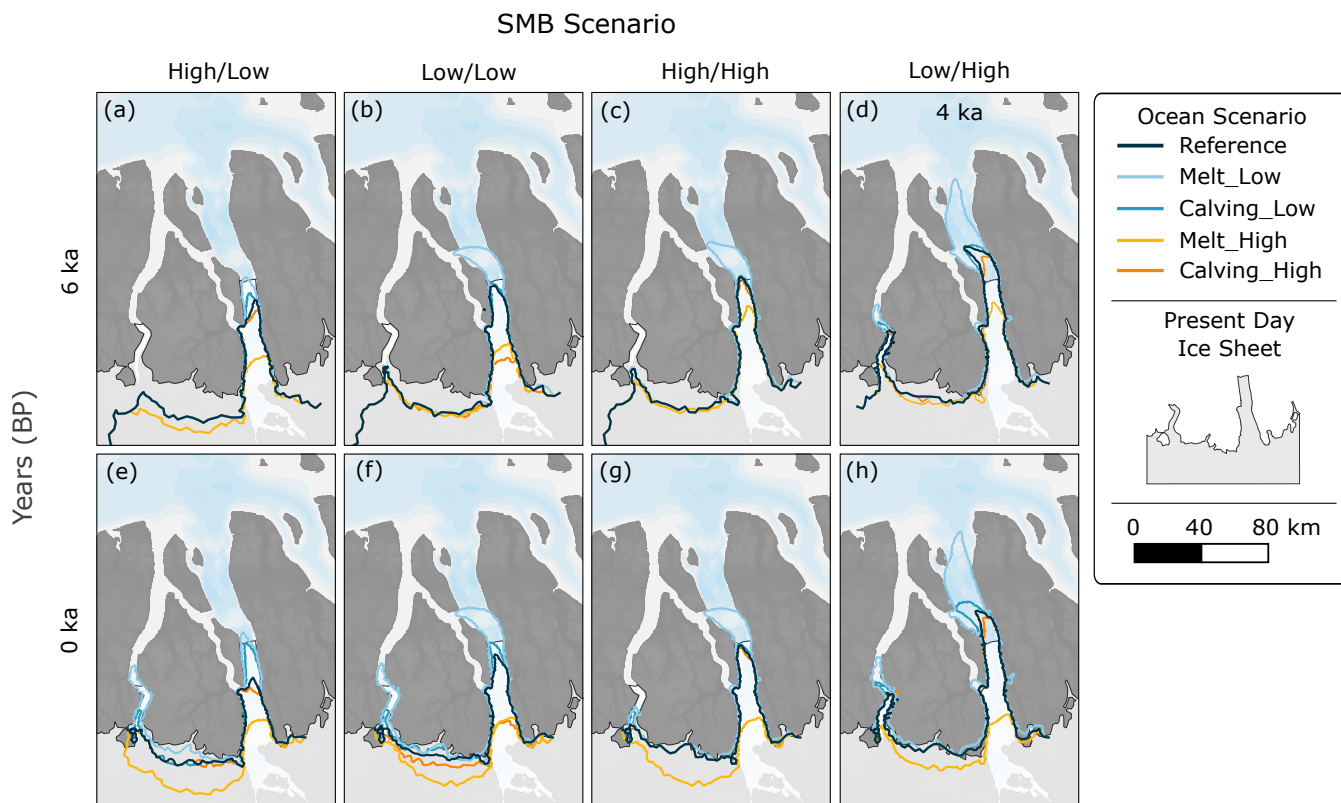
**Figure 10.** Comparison of the ice sheet margin at the Holocene minimum (**a-d**), and the end of our simulations representing present day (**e-h**). The various SMB scenarios are grouped into columns, while coloured ice sheet margins depict the ocean scenario used in each simulation: *Reference*: navy, *Melt_Low*: light blue, *Calving_Low*: blue, *Melt_High*: light orange and *Calving_High*: dark orange.

exposure event ages across the region. Nevertheless, the series of moraines that have been dated in Northern Greenland show a standstill in Holocene retreat between 9 and 8 ka BP and indicate that the ice sheet had not yet retreated behind its modern day extent (Fig. 1; Kelly and Bennike, 1992). This underscores that the retreat of the ice margin in the most negative SMB scenario High/Low is too pronounced, with the simulated ice margin already behind the present-day ice sheet by 9 ka BP.

### 4.2.2 Holocene minimum and regrowth

The minimum glaciated extent of the model domain during the transient Holocene runs is shown in Figure 10a-d. The terrestrial margin, on both Warming Land and Wulff Land, has retreated behind that of the present-day ice sheet in all simulations. There is little variation in the ice margin across the different ocean scenarios used for runs forced with Low/Low, High/High and Low/High SMB scenarios, with the simulated ice-sheet minimum sitting between 10 and 20 km behind the contemporary ice margin on Warming Land. For simulations using the High/Low SMB, modelled retreat is greater, with the margin retreated at

least 30 km behind the present-day ice sheet and Steensby Glacier withdrawing from St. George Fjord. Furthermore, simulation High/Low: *Melt_High* produces a retreat that is 10 km further in land than all other ocean forcings.

Regrowth of the terrestrial margin towards its present-day location occurs in all our simulations with the exception of those using the *Melt_High* ocean scenario (Fig. 10e-h). For such simulations, the ice-sheet margin remains almost unchanged from its Holocene minimum position, 20 - 40 km behind the present ice sheet depending on the chosen SMB scenario. All remaining runs using the High/High and Low/High SMB scenarios, both containing the high-precipitation pathway, end with an ice-sheet margin that is very consistent with the present-day ice sheet both across Warming Land and Wulff Land. For SMB scenarios High/Low and Low/Low there are variations in the final position of the ice front depending on the chosen ocean forcing; however, all simulations produced a final ice margin that is within 10 km of the contemporary ice sheet.

## 5   Discussion

We have simulated the Holocene evolution of Ryder Glacier across different plausible atmospheric- and oceanic-forcing scenarios with the glacier's terminus position and ice dynamics constrained by marine and terrestrial proxy records. In summary, we find that variations in SMB have a distinct impact on timings of retreat for both terrestrial and marine ice-sheet margins. The climate pathway built from low-temperature and high-precipitation (Low/High), matches the early Holocene terrestrial retreat across our domain best, in contrast to the most extreme scenario of high-temperature and low-precipitation (High/Low), which produces retreat that far exceeds the rate found in the terrestrial record (Fig. 9). For the marine margin of Ryder, enhanced ocean melt plays a key role in driving grounding-line retreat to match the sediment archive in all but the most extreme SMB scenario (Fig. 5). Moreover, ocean melt is crucial to initiate the collapse of Ryder's ice tongue in the HTM (Fig. 8), while the readvance of the grounding line towards its modern-day position only occurs with subdued ocean melt forcing (Fig. 5b). Furthermore, the variations in the calving threshold have a minimal impact during the early Holocene retreat, likely due to the continued presence of the floating tongue with its stability aided by the narrowing of Sherard Osborn Fjord. The major components influencing Ryder Glacier's behaviour in our simulations will be discussed in more detail below.

### 5.1   Holocene warming and the importance of precipitation

Atmospheric changes, associated with the pronounced shifts in surface temperatures and precipitation from the YD into the Holocene, exerted a first-order control on the behaviour of Ryder Glacier in our simulations. This is clear from the initial homogeneous retreat, >10 ka BP, found across all simulations in response to an abrupt rise in temperature and independent of the choice of ocean forcing. Subsequent variations in temperature and precipitation led to heterogenous retreat rates during the Holocene, yet the choice of SMB scenario provides a consistent pattern of retreat across all ocean forcings, ranging from the most extreme SMB scenario of high-temperature and low-precipitation to the mildest scenario of low-temperature and high-precipitation. We find that this mildest SMB scenario produces a terrestrial ice margin that fits best with reconstructed ice sheet positions in the geologic records (Fig. 9). Furthermore, precipitation exerts a substantial control in modulating mass loss during the early Holocene in our simulations, so much so that SMB scenarios using the low-precipitation pathways produce the

fastest retreat rates of both the grounding line and terrestrial ice margins (Fig. 5 and 9). This suggests that when the catchment of Ryder Glacier was deprived of snowfall, the grounding line retreated. These results contrast Holocene modelling studies of Southwestern Greenland, where variations in temperature played a greater role in determining retreat rates (Briner et al., 2020; Cuzzone et al., 2022).

We attribute the strong impact of precipitation during the Holocene to the environmental characteristics of Northern Greenland. The region, in its contemporary setting, experiences some of the lowest precipitation rates found on the ice sheet (Box, 2013; McIlhattan et al., 2020), owing to both its distance from major open water bodies, as the nearby Arctic Ocean is sea-ice covered, and to cooler temperatures at extreme latitudes. Consequently, Northern Greenland is especially vulnerable to rapid atmospheric warming (Noël et al., 2019). Reconstructed early Holocene precipitation suggests lower than modern rates of accumulation (Fig. 3b), hinting that North Greenland was highly sensitive to early Holocene warming. Biomarker analysis of sediment cores in the Lincoln Sea suggests that the period between about 11.3 and 9.7 ka BP may have experienced seasonal sea ice, implying nearby open-water conditions during summers (Detlef et al., 2023). However, it is not known whether such conditions in the Lincoln Sea directly affected precipitation over the North Greenland Ice Sheet. The sediment core study further suggests a maintained perennial sea-ice cover in the southern Lincoln Sea throughout the reminder of the Holocene. In contrast, towards the mid-Holocene, reduced sea-ice extent in Baffin Bay and the Labrador Sea, together with warmer temperatures, are thought to have brought greater than modern day levels of accumulation to Northern Greenland (Thomas et al., 2016). Such reasoning has been invoked to explain the readvance of valley glaciers and the sustained presence of local ice caps across Northern and Northeastern Greenland during the HTM (Möller et al., 2010; Larsen et al., 2016, 2019), while simulations of Hans Tausen Iskapp showed that precipitation rates higher than modern-day values were crucial in buffering higher temperatures during the HTM and ensuring the survival of the ice cap (Zekollari et al., 2017). Greater than modern-day precipitation rates are only found in our high-precipitation scenario (Fig 3b), which coupled with a low-temperature pathway produced the most accurate retreat of terrestrial margin during the early Holocene (Fig. 9).

## 5.2 Submarine melt drives inner fjord retreat

Whilst a negative trend in SMB is the overall dominant driver of Ryder Glacier's Holocene retreat, our results indicate that ice-ocean interactions played an increasingly important role as the interglacial progressed. The ocean melt rate is particularly important for the grounding line's retreat from the inner sill in Sherard Osborn Fjord, where our simulations produce a wide range of retreat dates spanning from 9.4 to 5.4 ka BP (Fig. 5). The study of O'Regan et al. (2021) shows that sedimentation on the inner sill, and thus the beginning of grounding line retreat, began at $9.3 \pm 0.4$ ka BP. We find that using a modern *Reference* ocean melt rate, our simulations are only able to match this timing of retreat when using the most negative SMB scenario (High/Low: *Reference*, Fig. 5a and 6e). Such an extreme SMB scenario leads to a terrestrial retreat that is significantly faster than that found in reconstructed isochrones (Fig. 9). Other, more moderate, SMB scenarios result in grounding-line evolutions lagging behind the sediment record when using *Reference* ocean melt forcings, with retreat from the inner sill not beginning until 8.3 ka BP (Fig. 5a and 6e). It is only when using a *High_Melt* ocean parameterisation that all SMB scenarios yield grounding-line retreats that are in line with the marine record (Fig. 5c and 6f).

The inner-sill has a ∼6.2 km wide central zone with a modern depth of ∼300 m (Jakobsson et al., 2020). Ocean melt rates at the grounding line atop the inner sill in our melt parametrisation would peak at 26.6 m yr$^{-1}$ for the *Reference* ocean scenario and 66.6 m yr$^{-1}$ for the *High_Melt* simulations, with the latter exceeding the modern melt rates seen under contemporary Greenlandic floating tongues with their grounding lines in much deeper waters (Wilson et al., 2017; Millan et al., 2023). Although the depth of the modern inner sill impedes the flow of warm AW (Jakobsson et al., 2020), relative sea-level (RSL) estimates from ∼8 ka BP indicate the sill to be between 40 and 80 m deeper than present (Lecavalier et al., 2014; Glueder et al., 2022), likely allowing AW to reach the paleo grounding line of Ryder Glacier, and drive higher melt rates that otherwise would not be possible in shallower, cooler waters. Cronin et al. (2022) discusses the evidence for the existence of such warm waters in the Lincoln Sea at the mouth of Sherard Osborn Fjord throughout the entire Holocene from a benthic ostracod and foraminifera assemblage. In particular, they point to a pronounced AW signal between 8.5 and 6 ka, which is close in time to the beginning of sedimentation on the inner sill. This stresses that the presence of warm AW in the fjord may have been crucial for the retreat of the grounding line from the sill. The presence of such warm waters around Greenland during the Holocene is well documented (Jennings et al., 2006; Pados-Dibattista et al., 2022), and has been indirectly linked to the collapse of the neighbouring Petermann Glacier's ice tongue during the HTM (Reilly et al., 2019). Furthermore, similar Holocene modelling studies at Jakobshavn Isbræ (Kajanto et al., 2020) and Northeast the Greenland Ice Stream (Tabone et al., 2024) also show that pronounced increases in ocean temperatures were required to force grounding line retreat from stable bathymetric highs in order to align with geological records.

Ocean melt rates were crucial to the stability of Ryder's floating tongue during the HTM. Our simulations produce a complete break-up of the ice tongue in two distinct manners: first during the early Holocene as the glacier retreats from the inner sill into deeper waters (Fig 7), second, during the mid-Holocene once the grounding line has already retreated into the shallower waters upstream of the present grounding line (Fig 8). The sediment facies that depict the collapse of Ryder's floating tongue, LU3 (6.3 ± 0.3 to 3.9 ± 0.4 ka BP), are dated ∼3 ka years after Ryder's retreat from the inner sill, LU5 (9.3 ± 0.4 to 7.6 ± 0.40 ka BP). The presence of LU4 (7.6 ± 0.40 to 6.3 ± 0.3 ka BP), a faintly laminated facies that lacks evidence of bioturbation, suggests that Ryder maintained its floating tongue for a substantial period of time as the grounding line retreated away from the inner sill (O'Regan et al., 2021). We therefore argue that the collapse of Ryder's tongue is best captured in runs using the *High_Melt* scenario, wherein Ryder retreats steadily through the over-deepened part of the fjord behind the inner sill, while continuing to be buttressed by a floating tongue, towards its Holocene minimum position. In this scenario, elevated melt rates result in a shortened floating tongue that weakens the glacier's ability to buttress interior ice, thus driving an increase in ice velocities and calving until its eventual collapse (Fig. 8).

## 5.3 Ryder's floating tongue was pivotal in its Holocene evolution

Mass loss through calving has played a key role in the recent evolution of the GrIS and is projected to play a vital role in the coming century (Goelzer et al., 2020; Choi et al., 2021). Yet, such processes are often not explicitly included in paleo-modelling efforts owing to the computational costs associated with high-resolution grids needed to accurately simulate fast flowing ice streams and their associated calving dynamics. Here, we build on the findings of Cuzzone et al. (2022), who

included a similar calving setup when simulating the Holocene retreat of Kangiata Nunaata Sermia, South Western Greenland. Cuzzone et al. (2022) note how the inclusion of calving allowed the marine margins to persist longer in the fjords, relative to adjacent terrestrial ice, due to a greater transport of mass from the interior, which in turn led to thinning in the upper regions of the domain. We find such consistencies across our simulations during the early Holocene, where, despite rapid retreat of the
485 terrestrial ice, Ryder Glacier maintains an extended position in the fjord (Fig. 9).

In our simulations, variations to the calving threshold have minimal influence on the grounding line evolution and inland thinning of Ryder Glacier (Fig. 5a, d and e; and Fig. A3). We attribute this to the sustained presence of an ice tongue during the Holocene retreat, suppressing calving and discharge. When we simulate a collapse of the ice tongue, either during retreat from the inner sill (Fig. 7) or at Ryder's Holocene minimum (Fig. 8), the loss of buttressing and transition to calving from
490 an unconstrained grounded front leads to an increase in ice discharge and inland thinning. Our results indicate that Ryder's floating tongue was present during the entire >4,000 year retreat from the outer sill, stabilising the glacier and modulating ice discharge until its collapse at the glacier's Holocene minimum position. This long-term stability was likely supported by the geometry of Sherard Osborn Fjord, which continually narrows from the outer sill towards a 10 km wide bottleneck that extends 40 km south from the inner sill (Fig. 2). This region has been linked to the stability of the contemporary ice tongue and
495 calving front (Holmes et al., 2021), where narrowing fjord walls increase lateral drag, modulating grounding line retreat and, crucially, floating tongue stability (Åkesson et al., 2018b; Frank et al., 2022). The bottleneck likely allowed Ryder's ice tongue to outlast the floating extension at the neighbouring Petermann Glacier, which collapsed at 6.9 ka BP only ∼600 years into the glacier's retreat from the outer sill in Petermann Fjord after which the fjord's geometry begins to deepen and, crucially, widen (Reilly et al., 2019). With the collapse of Nioghalvfjerdsbræ (79N) occurring even earlier, by 8.5 ka BP (Smith et al., 2023),
500 it is very likely that Sherard Osborn Fjord contained the last major floating extension from the Greenland Ice Sheet during the deglaciation from the LGM.

The heightened discharge from a collapse of the floating ice tongue at Ryder restricts any re-advance of both the terrestrial and marine margins during the late Holocene (Fig. 6n and 10). This implies that a shift in calving dynamics, driven by the regrowth of the ice tongue and increased buttressing, was crucial to the re-advance of Ryder glacier during the late Holocene.
505 Although our experimental set-up does not account for transiently evolving ocean forcings, the lack of ice-tongue regrowth across all SMB scenarios indicates that cooling atmospheric temperatures alone are not sufficient for the regrowth of the floating terminus, and that a reduction in ocean melt rate and/or a reduction in calving owing to the formation of a rigid ice mélange was required. This aligns with the results of Åkesson et al. (2022) who found that a decrease in both ocean melt and calving was required to regrow Petermann Glacier's ice tongue in the event of any collapse as well as work by Kajanto et al. (2024),
510 where a decrease in calving rate was required to re-form the ice tongue of Jakobshavn Isbræ and readvance the grounding line to the glacier's LIA position.

Our findings emphasise the role of floating tongues in controlling ice discharge over centennial and millennial time scales and stress the importance of both including floating ice and calving dynamics when undertaking paleo-modelling studies of the GrIS. This is especially pertinent to Northern Greenland, where ice streams at the LGM were thought to have coalesced
515 and formed ice shelf conditions into the Lincoln Sea (Dawes, 1986; Larsen et al., 2010) before collapsing during the HTM and

then regrowing in the late Holocene to exert an important buttressing force on ice flow from the GrIS interior. Continental-scale model reconstructions of the GrIS during the Holocene which omit the inclusion of floating ice and calving, or do not have the required model resolution to capture grounding line dynamics in narrow Greenlandic fjords, may lack the required fidelity to accurately simulate the ice-sheet's evolution (Simpson et al., 2009; Lecavalier et al., 2014).

520    While we have discussed the importance of fjord geometry and bathymetry to the evolution of Ryder Glacier, we acknowledge that one of the limitations of our experimental set-up is lack of transient RSL changes during the Holocene. Despite this, we tentatively assume that including such dynamics would not have a significant impact on our model results, taking note from a similar Holocene study of Jakobshavn Isbræ by Kajanto et al. (2020), which found RSL changes had minimal impact on the in-fjord retreat as such variations are small compared to fjord depth. Although the coalescing of the Greenland and Innuitian ice sheets brought RSL ∼80 m higher at the beginning of the Holocene (Lecavalier et al., 2014; Glueder et al., 2022), the pronounced depths of Sherard Osborn Fjord mean it is likely that any influence would have been restricted to the shallow inner sill as discussed in Section 5.2. Future work, which will aim to simulate the Holocene deglaciation of the entire northern sector of the GrIS, will include RSL variations through new solid earth feedbacks currently being implemented in ISSM or through prescribed forcings of sea level changes from prior research (e.g. Caron et al., 2018).

## 5.4    Ryder Glacier in the future

The retreat of Ryder to its HTM minimum provides a crucial analogue to understand how the glacier will evolve when confronted with sustained temperatures above pre-industrial levels. Our simulations indicate that both atmospheric- and ocean-ice interactions will dictate Ryder's future behaviour. At present, Ryder's floating tongue and grounding line sit within the bottleneck of Sherard Osborn Fjord, providing significant buttressing and stability. The calving front has remained unmoved for half a century, owing to fjord geometry (Holmes et al., 2021). If the ice tongue at Ryder persists, the grounding line will undergo a steady retreat along the prograde topography inland of its current position, with the speed of retreat a function of both SMB and submarine melt, with the latter able to weaken the floating tongue's ability to buttress leading to enhanced discharge (Fig. 8). Despite being shielded from warm AW by the shallower inner sill (Jakobsson et al., 2020), melt rates at the grounding line of Ryder have increased in recent decades while the floating tongue has thinned (Millan et al., 2023). Submarine melt is not just a product of ocean heat, but also turbulent processes at the ice-ocean interface that are linked to the upwelling of buoyant plumes fed by the discharge of fresh water at the grounding line (Slater and Straneo, 2022). At Nioghalvfjerdsbræ(79N), Greenland's largest floating terminus that is also shielded from warm AW by a bathymetric high (Hill et al., 2017; An et al., 2021), extreme melt rates of 100 m yr$^{-1}$ have been linked to increased subglacial discharge from enhanced surface melt (Zeising et al., 2024). Rising melt rates at Ryder has coincided with a substantial increase in supraglacial lakes on the glacier (Otto et al., 2022), the build-up and drainage of which are likely to deliver an increased flux of fresh water to the grounding line that will lead to a greater transfer of heat from the ocean to the glacier. Therefore, despite the protection offered by the inner-sill in Sherard Osborn Fjord, ocean melt is set to play a crucial role in both the grounding line retreat and tongue stability of Ryder Glacier into the future.

During the HTM Ryder retreated inland of its present position. The most common Holocene minimum position achieved in our simulations is ∼25 km behind the modern-day grounding line, in relatively shallow waters (∼300 m deep) and in front of the restricted embayment (Fig. 6 and 8). The ever decreasing marine ice thickness heightens the role of atmospheric-ice interaction and indicates that further retreat would require a greater negative trend in SMB. This is best exemplified in both runs that use the extreme *High* ocean forcing which retreat to their Holocene marine minimum by 9 ka BP (Fig. 6h), only to remain unmoved during the HTM. While we are unable to match the grounding-line retreat into the restricted embayment hypothesised by O'Regan et al. (2021), the inherent uncertainties in SMB reconstructions over the Holocene mean that further retreat from our simulated position cannot be ruled out in a HTM like climate. However, owing to the substantial thickness of simulated inland ice, we believe that it is unlikely that Ryder retreated significantly further and became entirely terrestrial during the Holocene. Instead, it appears that Ryder remained a marine terminating glacier during the HTM, with the grounding line in shallow waters in front of or in the restricted embayment. This implies that under a future climate that resembles the HTM, Ryder will retain its connection to the ocean and will continue to contribute to global sea level rise through both runoff and discharge.

## 6   Conclusions

Geological evidence from terrestrial and marine settings can provide valuable insights into the evolution of ice sheets across glacial/interglacial cycles at snapshots in time. Coupling such knowledge with ice-sheet models allows for continuous insight into the long-term evolution of ice sheets. Here, we employed a high-resolution 3D thermomechanical ice sheet model to explore the evolution of Ryder Glacier throughout the Holocene. By focusing on a single outlet glacier from the GrIS, we were able to run our model at mesh resolutions under <1 km to both accurately simulate grounding line dynamics and disentangle the influence of ice-ocean and ice-atmosphere interactions. We find that:

- Rapid retreat of the ice margin in the early Holocene was driven by substantial climatic warming. The retreat of both the terrestrial and marine ice margins is independent of the prescribed ocean forcing during the transition out of the YD until ∼10 ka BP.

- Precipitation rates played a key role in modulating both the pace and magnitude of retreat, likely reflecting the arid nature of Northern Greenland. We find that the climate scenario where mid-Holocene precipitation rates exceed that of contemporary levels produces terrestrial ice retreat that best matches the geologic record.

- After ∼10 ka BP, submarine melt begins to influence the retreat of the marine margin of Ryder Glacier in all but the most negative SMB scenario. Heightened submarine melt rates were crucial in retreating Ryder from a stable position on the inner sill as well as inducing the collapse of the ice tongue during the HTM.

- Before its collapse, the paleo-ice tongue at Ryder Glacier was crucial in modulating ice loss during the early Holocene, particularly during Ryder's retreat from the inner sill into a large overdeepening in Sherard Osborn Fjord. We link the

580 ice tongue's stability and influence to the 10 km wide bottleneck in Sherard Osborn, where the contemporary ice tongue and grounding line currently lie.

   – Re-growth of the ice tongue was crucial to the readvance of both the terrestrial and marine ice margins during the late Holocene cooling. Changes in SMB alone cannot explain the re-formation of the tongue, indicating that cooling ocean temperatures and reduced calving rates were required.

585 Although changes in SMB may dictate large-scale ebbs and flows in ice-sheet margins, ice-ocean interactions can play a significant role in the evolution of marine outlet glaciers, and thus discharge from ice sheets, across extended timescales of centuries and millennia. By running Holocene simulations of Ryder Glacier we provide vital analogues for the future evolution of the glacier in a warming climate, stressing both the continued importance of the ice tongue in buttressing ice flow and the role of submarine melt in weakening the ice tongue and driving grounding line retreat.

590 *Code availability.* All the code necessary for running simulations using ISSM is freely available at https://issm.jpl.nasa.gov/download/ .

**Appendix A**

**A1**

Here we test whether the Von Mises calving law with $\sigma_{max}$ value of 300 kPa (Eq. 4), found to be a suitable tuning value for the neighbouring Petermann Glacier (Åkesson et al., 2022), reproduces the contemporary evolution of Ryder Glacier's terminus.
595 To do this, we run our ice sheet model from 2008 forward to 2025 and compare the position of the ice front to observations. The initial ice front position and ice geometry are taken from BedMachine v3 which has a nominal date of 2008 (Morlighem et al., 2017). Figure A1 shows the position of the observed front in 2025 against our simulated front using the Von Mises law with a $\sigma_{max}$ value of 300 kPa. The calving law reproduces the 2025 position well capturing the overall trend of glacier advance during the 17 years. Although the centre of the ice tongue terminus is slightly too advanced, its margins, and their connection
600 to the fjord walls which offer buttressing, terminate in a similar position to that observed in 2025
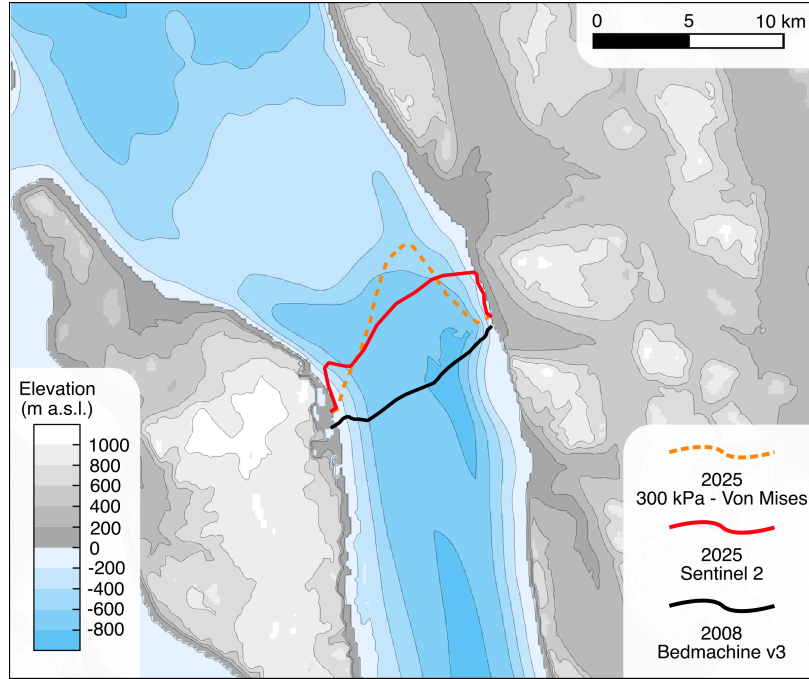
**Figure A1.** A comparison between the recent observed evolution of Ryder's calving front with a simulated front using the Von Mises calving law. The 2008 position of Ryder's terminus (black) is sourced from BedMachine v3 (Morlighem et al., 2017) and is taken as the initial ice front position for our comparison simulation. The 2025 position of Ryder's terminus (red) is taken from a Sentinel 2 satellite image dated 19-05-2025. The simulated 2025 position of Ryder (dashed orange) uses the Von Mises calving law with a threshold of 300 kPa. Surface topography and ocean bathymetry are from BedMachine v5 (Morlighem et al., 2022).
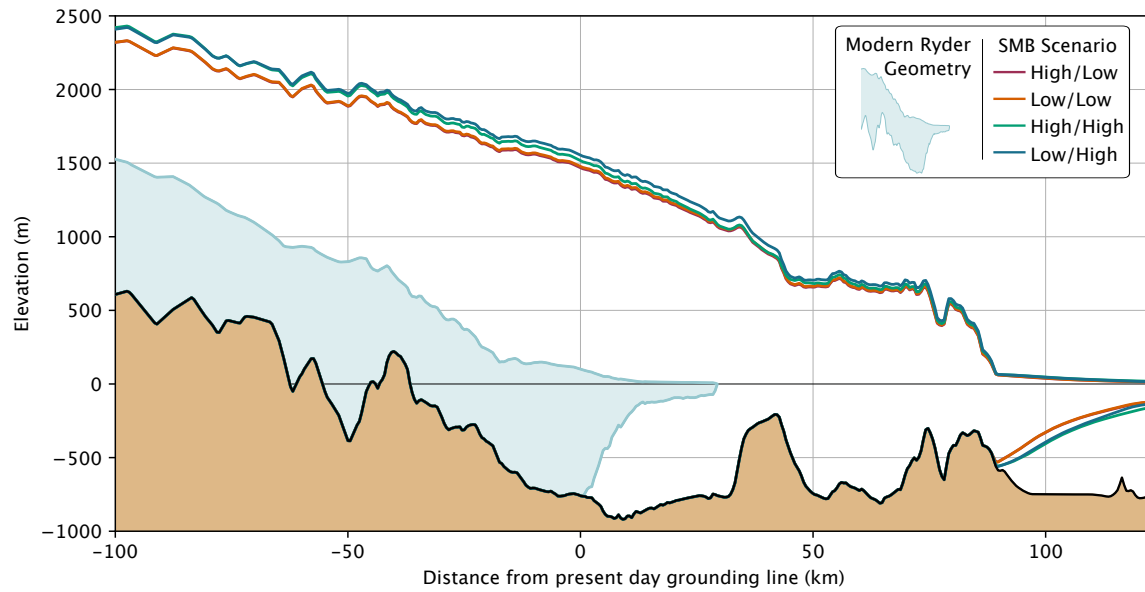
**Figure A2.** A comparison between the geometry of the present day Ryder Glacier (light blue) and that of the glacier after running a 20,000 year spin-up forced with a YD climate for the differing SMB scenarios: High/Low (red), Low/Low (Orange), High/High (Green) and Low/High (Blue). Bedrock data and the present day ice surface is from BedMachine v5 (Morlighem et al., 2022).
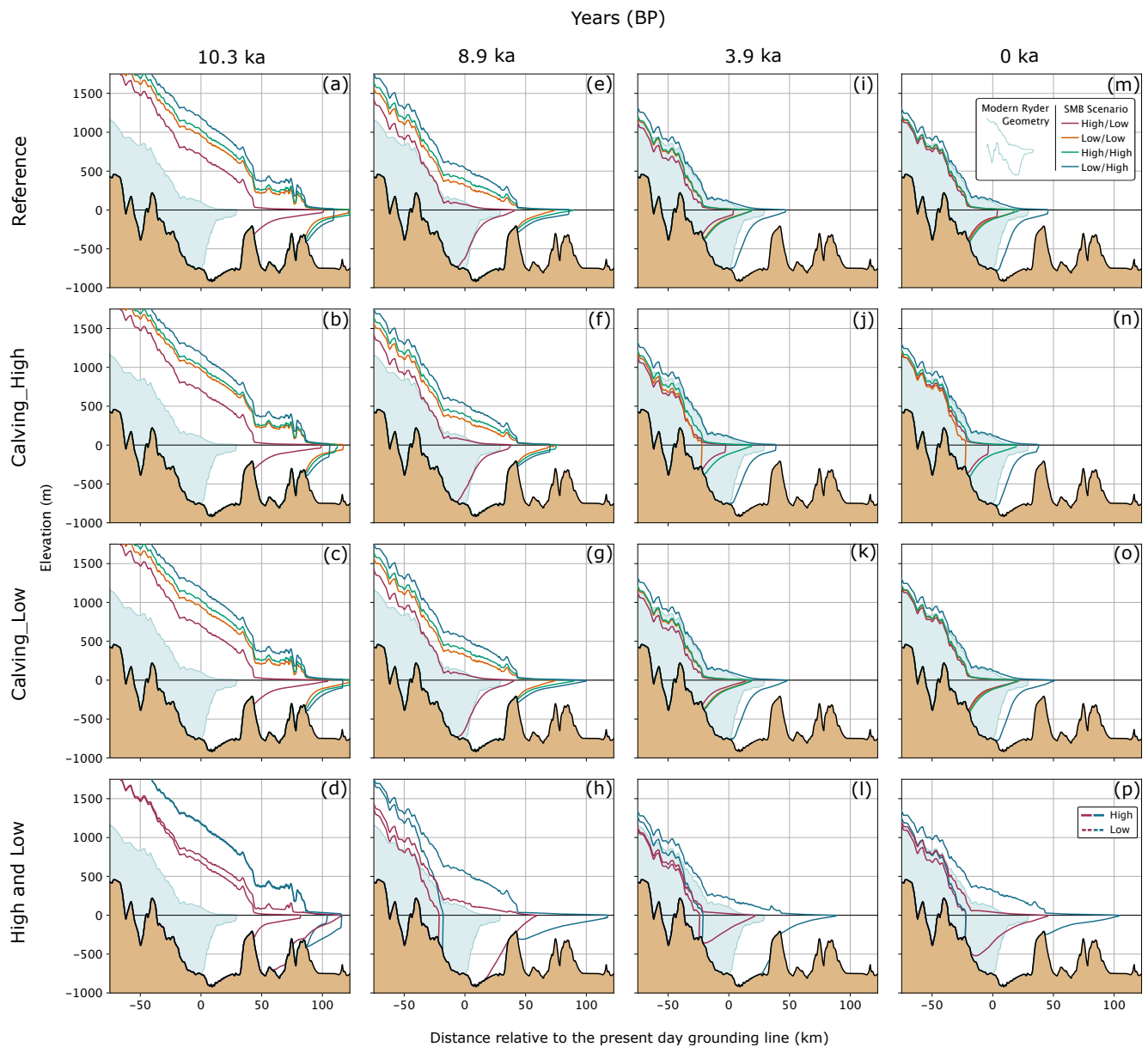
**Figure A3.** Evolution of Ryder Glacier in 2D cross section views along the centre flowline during the Holocene at specific time stamps. Dates of 10.3 ka **(a-d)**, 8.9 ka **(e-h)**, 3.9 ka **(i-l)** and 0 ka **(m-p)**, represent specific landmarks in the evolution of Ryder as discussed in O'Regan et al. (2021). Each row represents a different ocean forcing used in the transient simulation (Table 1), from top down this includes: *Reference*, *Calving_High*, *Calving_Low* and both extreme *High* and *Low* Scenarios. Each plot contains the 4 different SMB scenarios: High/Low (red), Low/Low (Orange), High/High (Green) and Low/High (Blue).
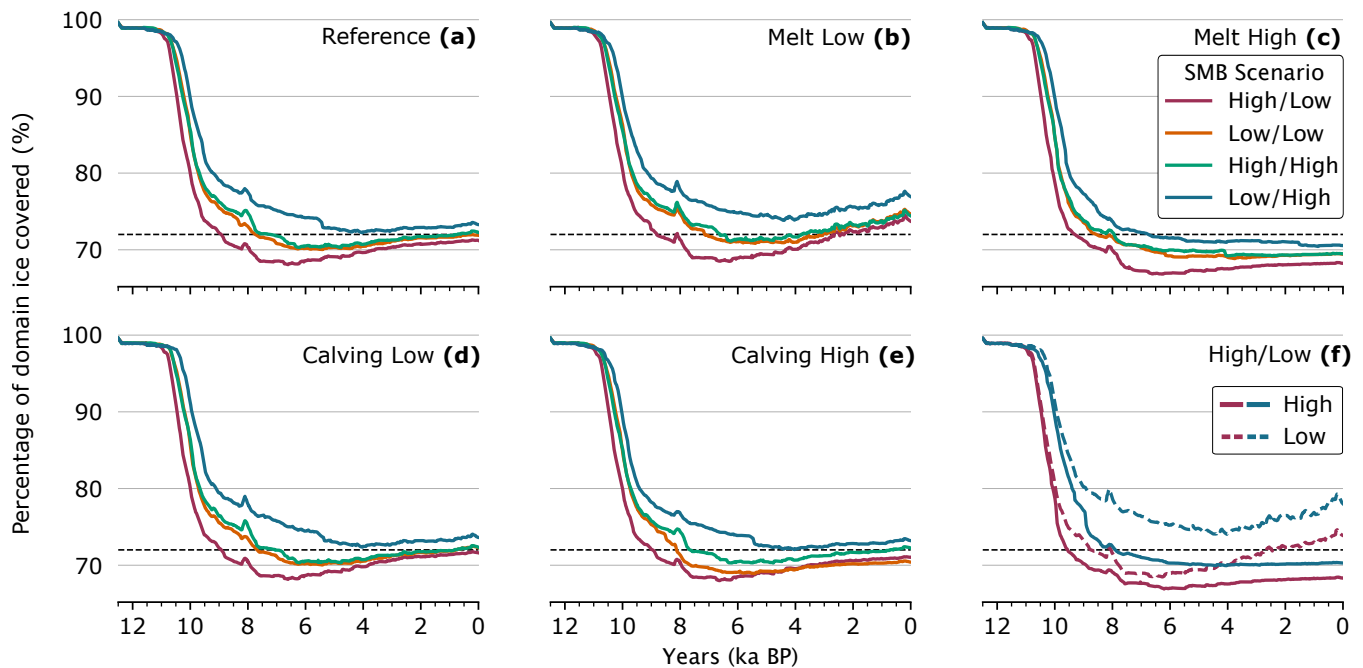
**Figure A4.** Evolution of ice cover in the model domain during the Holocene simulations. Line colour defines the SMB scenario for the transient runs: High/Low (red), Low/Low (Orange), High/High (Green) and Low/High (Blue). Each subplot represents a different ocean scenario: **(a)** *Reference*, **(b)** *Melt_Low*, **(c)** *Melt_High*, **(d)** *Calving_Low*, **(e)** *Calving_High* and **(f)** both the extreme *High* and *Low* ocean forcings. The dashed black line represent the contemporary percentage of the domain covered with ice, 72%.

*Author contributions.* The study was conceived by JB and MJ. JB ran all model simulations with technical advice from FAH, JC, HA and MM. JB completed data analysis on all simulations with the interpretation of results discussed amongst all authors. The manuscript was written by JB with significant input from all authors.

*Competing interests.* The authors declare no competing interests.

605 *Acknowledgements.* All simulation were conducted using resources provided by the National Academic Infrastructure for Supercomputing in Sweden (NAISS) at the National Supercomputer Centre at Linköping University, Sweden, partially funded by the Swedish Research Council through grant agreement no. 2022-06725. JB was funded by VR Grant no. 2021-04512 and FAH was funded by Formas Grant no. 2021-01590, both awarded to MJ. HÅ was supported by the project JOSTICE from the Research Council of Norway (grant no. 302458) and ERC-2022-ADG grant agreement No 01096057 GLACMASS from the European Research Council. JN was funded by VR grant no. 610 2020-05076. NK was funded by VR grant no. 2022-03718. MO was funded by VR grant no. 2020-04379. JC was funded by NSF Office of Polar Programs grant no. 2106971. The authors are grateful to both the editor and two anonymous reviewers for their comments and suggestions concerning earlier versions of the manuscript.

# References

Amaral, T., Bartholomaus, T. C., and Enderlin, E. M.: Evaluation of Iceberg Calving Models Against Observations From Greenland Outlet Glaciers, Journal of Geophysical Research: Earth Surface, 125, e2019JF005 444, https://doi.org/10.1029/2019JF005444, 2020.

An, L., Rignot, E., Wood, M., Willis, J. K., Mouginot, J., and Khan, S. A.: Ocean melting of the Zachariae Isstrøm and Nioghalvfjerdsfjorden glaciers, northeast Greenland, Proceedings of the National Academy of Sciences, 118, e2015483 118, https://doi.org/10.1073/pnas.2015483118, 2021.

Aschwanden, A., Bueler, E., Khroulev, C., and Blatter, H.: An enthalpy formulation for glaciers and ice sheets, Journal of Glaciology, 58, 441–457, https://doi.org/10.3189/2012JoG11J088, publisher: Cambridge University Press, 2012.

Badgeley, J. A., Steig, E. J., Hakim, G. J., and Fudge, T. J.: Greenland temperature and precipitation over the last 20000 years using data assimilation, Climate of the Past, 16, 1325–1346, https://doi.org/10.5194/cp-16-1325-2020, publisher: Copernicus GmbH, 2020.

Blatter, H.: Velocity and stress fields in grounded glaciers: a simple algorithm for including deviatoric stress gradients, Journal of Glaciology, 41, 333–344, https://doi.org/10.3189/S002214300001621X, 1995.

Bondzio, J. H., Seroussi, H., Morlighem, M., Kleiner, T., Rückamp, M., Humbert, A., and Larour, E. Y.: Modelling calving front dynamics using a level-set method: application to Jakobshavn Isbræ, West Greenland, The Cryosphere, 10, 497–510, https://doi.org/10.5194/tc-10-497-2016, publisher: Copernicus GmbH, 2016.

Born, A. and Nisancioglu, K. H.: Melting of Northern Greenland during the last interglaciation, The Cryosphere, 6, 1239–1250, https://doi.org/10.5194/tc-6-1239-2012, publisher: Copernicus GmbH, 2012.

Box, J. E.: Greenland Ice Sheet Mass Balance Reconstruction. Part II: Surface Mass Balance (1840–2010), Journal of Climate, 26, 6974–6989, https://doi.org/10.1175/JCLI-D-12-00518.1, publisher: American Meteorological Society Section: Journal of Climate, 2013.

Box, J. E., Hubbard, A., Bahr, D. B., Colgan, W. T., Fettweis, X., Mankoff, K. D., Wehrlé, A., Noël, B., van den Broeke, M. R., Wouters, B., Bjørk, A. A., and Fausto, R. S.: Greenland ice sheet climate disequilibrium and committed sea-level rise, Nature Climate Change, 12, 808–813, https://doi.org/10.1038/s41558-022-01441-2, publisher: Nature Publishing Group, 2022.

Braithwaite, R. J.: Positive degree-day factors for ablation on the Greenland ice sheet studied by energy-balance modelling, Journal of Glaciology, 41, 153–160, https://doi.org/10.3189/S0022143000017846, 1995.

Briner, J. P., McKay, N. P., Axford, Y., Bennike, O., Bradley, R. S., de Vernal, A., Fisher, D., Francus, P., Fréchette, B., Gajewski, K., Jennings, A., Kaufman, D. S., Miller, G., Rouston, C., and Wagner, B.: Holocene climate change in Arctic Canada and Greenland, Quaternary Science Reviews, 147, 340–364, https://doi.org/10.1016/j.quascirev.2016.02.010, 2016.

Briner, J. P., Cuzzone, J. K., Badgeley, J. A., Young, N. E., Steig, E. J., Morlighem, M., Schlegel, N.-J., Hakim, G. J., Schaefer, J. M., Johnson, J. V., Lesnek, A. J., Thomas, E. K., Allan, E., Bennike, O., Cluett, A. A., Csatho, B., de Vernal, A., Downs, J., Larour, E., and Nowicki, S.: Rate of mass loss from the Greenland Ice Sheet will exceed Holocene values this century, Nature, 586, 70–74, https://doi.org/10.1038/s41586-020-2742-6, number: 7827 Publisher: Nature Publishing Group, 2020.

Budd, W. F., Keage, P. L., and Blundy, N. A.: Empirical Studies of Ice Sliding, Journal of Glaciology, 23, 157–170, https://doi.org/10.3189/S0022143000029804, publisher: Cambridge University Press, 1979.

Caron, L., Ivins, E. R., Larour, E., Adhikari, S., Nilsson, J., and Blewitt, G.: GIA Model Statistics for GRACE Hydrology, Cryosphere, and Ocean Science, Geophysical Research Letters, 45, 2203–2212, https://doi.org/10.1002/2017GL076644, _eprint: https://onlinelibrary.wiley.com/doi/pdf/10.1002/2017GL076644, 2018.

Choi, Y., Morlighem, M., Wood, M., and Bondzio, J. H.: Comparison of four calving laws to model Greenland outlet glaciers, The Cryosphere, 12, 3735–3746, https://doi.org/10.5194/tc-12-3735-2018, 2018.

Choi, Y., Morlighem, M., Rignot, E., and Wood, M.: Ice dynamics will remain a primary driver of Greenland ice sheet mass loss over the next century, Communications Earth & Environment, 2, 26, https://doi.org/10.1038/s43247-021-00092-z, 2021.

Courant, R., Friedrichs, K., and Lewy, H.: Über die partiellen Differenzengleichungen der mathematischen Physik, Mathematische Annalen, 100, 32–74, https://doi.org/10.1007/BF01448839, 1928.

Cronin, T. M., Olds, B. M., Regnier, A. M., O'Regan, M., Gemery, L., Detlef, H., Pearce, C., and Jakobsson, M.: Holocene paleoceanography and glacial history of Lincoln Sea, Ryder Glacier, Northern Greenland, based on foraminifera and ostracodes, Marine Micropaleontology, 175, 102 158, https://doi.org/10.1016/j.marmicro.2022.102158, 2022.

Cuffey, K. and Paterson, W. S. B.: The physics of glaciers, Butterworth-Heinemann/Elsevier, Burlington, MA, 4th ed edn., ISBN 978-0-12-369461-4, oCLC: ocn488732494, 2010.

Cuzzone, J. K., Morlighem, M., Larour, E., Schlegel, N., and Seroussi, H.: Implementation of higher-order vertical finite elements in ISSM v4.13 for improved ice sheet flow modeling over paleoclimate timescales, Geoscientific Model Development, 11, 1683–1694, https://doi.org/10.5194/gmd-11-1683-2018, publisher: Copernicus GmbH, 2018.

Cuzzone, J. K., Schlegel, N.-J., Morlighem, M., Larour, E., Briner, J. P., Seroussi, H., and Caron, L.: The impact of model resolution on the simulated Holocene retreat of the southwestern Greenland ice sheet using the Ice Sheet System Model (ISSM), The Cryosphere, 13, 879–893, https://doi.org/10.5194/tc-13-879-2019, publisher: Copernicus GmbH, 2019.

Cuzzone, J. K., Young, N. E., Morlighem, M., Briner, J. P., and Schlegel, N.-J.: Simulating the Holocene deglaciation across a marine-terminating portion of southwestern Greenland in response to marine and atmospheric forcings, The Cryosphere, 16, 2355–2372, https://doi.org/10.5194/tc-16-2355-2022, publisher: Copernicus GmbH, 2022.

Davis, P. T., Menounos, B., and Osborn, G.: Holocene and latest Pleistocene alpine glacier fluctuations: a global perspective, Quaternary Science Reviews, 28, 2021–2033, https://doi.org/10.1016/j.quascirev.2009.05.020, 2009.

Dawes, P. R.: Geological photo-interpretation of Hall Land: part of the regional topographical-geological mapping of northern Greenland, Rapport Grønlands Geologiske Undersøgelse, 85, 25–30, https://doi.org/10.34194/rapggu.v85.7522, 1977.

Dawes, P. R.: Glacial erratics on the Arctic Ocean margin of North Greenland: implications for an extensive ice-shelf, Bulletin of the Geological Society of Denmark, 35, 59–69, https://doi.org/10.37570/bgsd-1986-35-07, 1986.

Detlef, H., O'Regan, M., Stranne, C., Jensen, M. M., Glasius, M., Cronin, T. M., Jakobsson, M., and Pearce, C.: Seasonal sea-ice in the Arctic's last ice area during the Early Holocene, Communications Earth & Environment, 4, 86, https://doi.org/10.1038/s43247-023-00720-w, 2023.

Enderlin, E. M., Howat, I. M., Jeong, S., Noh, M.-J., van Angelen, J. H., and van den Broeke, M. R.: An improved mass budget for the Greenland ice sheet, Geophysical Research Letters, 41, 866–872, https://doi.org/10.1002/2013GL059010, 2014.

England, J.: Coalescent Greenland and Innuitian ice during the Last Glacial Maximum: revising the Quaternary of the Canadian High Arctic, Quaternary Science Reviews, 18, 421–456, https://doi.org/10.1016/S0277-3791(98)00070-5, 1999.

England, J., Atkinson, N., Bednarski, J., Dyke, A. S., Hodgson, D. A., and Ó Cofaigh, C.: The Innuitian Ice Sheet: configuration, dynamics and chronology, Quaternary Science Reviews, 25, 689–703, https://doi.org/10.1016/j.quascirev.2005.08.007, 2006.

Fettweis, X., Hofer, S., Krebs-Kanzow, U., Amory, C., Aoki, T., Berends, C. J., Born, A., Box, J. E., Delhasse, A., Fujita, K., Gierz, P., Goelzer, H., Hanna, E., Hashimoto, A., Huybrechts, P., Kapsch, M.-L., King, M. D., Kittel, C., Lang, C., Langen, P. L., Lenaerts, J. T. M., Liston, G. E., Lohmann, G., Mernild, S. H., Mikolajewicz, U., Modali, K., Mottram, R. H., Niwano, M., Noël, B., Ryan, J. C., Smith, A.,

Streffing, J., Tedesco, M., van de Berg, W. J., van den Broeke, M., van de Wal, R. S. W., van Kampenhout, L., Wilton, D., Wouters, B., Ziemen, F., and Zolles, T.: GrSMBMIP: intercomparison of the modelled 1980–2012 surface mass balance over the Greenland Ice Sheet, The Cryosphere, 14, 3935–3958, https://doi.org/10.5194/tc-14-3935-2020, publisher: Copernicus GmbH, 2020.

690   Frank, T., Åkesson, H., De Fleurian, B., Morlighem, M., and Nisancioglu, K. H.: Geometric controls of tidewater glacier dynamics, The Cryosphere, 16, 581–601, https://doi.org/10.5194/tc-16-581-2022, 2022.

Funder, S. and Larsen, O.: Implications of volcanic erratics in Quaternary deposits of North Greenland., Bulletin of the Geological Society of Denmark, 31, 57–61, https://doi.org/10.37570/bgsd-1982-31-05, 1982.

Funder, S., Goosse, H., Jepsen, H., Kaas, E., Kjær, K. H., Korsgaard, N. J., Larsen, N. K., Linderson, H., Lyså, A., Möller, P., Olsen,

695   J., and Willerslev, E.: A 10,000-Year Record of Arctic Ocean Sea-Ice Variability—View from the Beach, Science, 333, 747–750, https://doi.org/10.1126/science.1202760, 2011.

Glueder, A., Mix, A. C., Milne, G. A., Reilly, B. T., Clark, J., Jakobsson, M., Mayer, L., Fallon, S. J., Southon, J., Padman, J., Ross, A., Cronin, T., and McKay, J. L.: Calibrated relative sea levels constrain isostatic adjustment and ice history in northwest Greenland, Quaternary Science Reviews, 293, 107 700, https://doi.org/10.1016/j.quascirev.2022.107700, 2022.

700   Goelzer, H., Nowicki, S., Payne, A., Larour, E., Seroussi, H., Lipscomb, W. H., Gregory, J., Abe-Ouchi, A., Shepherd, A., Simon, E., Agosta, C., Alexander, P., Aschwanden, A., Barthel, A., Calov, R., Chambers, C., Choi, Y., Cuzzone, J., Dumas, C., Edwards, T., Felikson, D., Fettweis, X., Golledge, N. R., Greve, R., Humbert, A., Huybrechts, P., Le clec'h, S., Lee, V., Leguy, G., Little, C., Lowry, D. P., Morlighem, M., Nias, I., Quiquet, A., Rückamp, M., Schlegel, N.-J., Slater, D. A., Smith, R. S., Straneo, F., Tarasov, L., van de Wal, R., and van den Broeke, M.: The future sea-level contribution of the Greenland ice sheet: a multi-model ensemble study of ISMIP6, The Cryosphere, 14,

705   3071–3096, https://doi.org/10.5194/tc-14-3071-2020, 2020.

He, F., Shakun, J. D., Clark, P. U., Carlson, A. E., Liu, Z., Otto-Bliesner, B. L., and Kutzbach, J. E.: Northern Hemisphere forcing of Southern Hemisphere climate during the last deglaciation, Nature, 494, 81–85, https://doi.org/10.1038/nature11822, publisher: Nature Publishing Group, 2013.

Hill, E. A., Carr, J. R., and Stokes, C. R.: A Review of Recent Changes in Major Marine-Terminating Outlet Glaciers in Northern Greenland,

710   Frontiers in Earth Science, 4, https://www.frontiersin.org/articles/10.3389/feart.2016.00111, 2017.

Hill, E. A., Carr, J. R., Stokes, C. R., and Gudmundsson, G. H.: Dynamic changes in outlet glaciers in northern Greenland from 1948 to 2015, The Cryosphere, 12, 3243–3263, https://doi.org/10.5194/tc-12-3243-2018, publisher: Copernicus GmbH, 2018a.

Hill, E. A., Gudmundsson, G. H., Carr, J. R., and Stokes, C. R.: Velocity response of Petermann Glacier, northwest Greenland, to past and future calving events, The Cryosphere, 12, 3907–3921, https://doi.org/10.5194/tc-12-3907-2018, 2018b.

715   Holmes, F., Kirchner, N., Prakash, A., Stranne, C., Dijkstra, S., and Jakobsson, M.: Calving at Ryder Glacier, Northern Greenland, Journal of Geophysical Research: Earth Surface, 126, https://doi.org/10.1029/2020JF005872, 2021.

Humbert, A., Helm, V., Neckel, N., Zeising, O., Rückamp, M., Khan, S. A., Loebel, E., Brauchle, J., Stebner, K., Gross, D., Sonder-shaus, R., and Müller, R.: Precursor of disintegration of Greenland's largest floating ice tongue, The Cryosphere, 17, 2851–2870, https://doi.org/10.5194/tc-17-2851-2023, publisher: Copernicus GmbH, 2023.

720   Jakobsson, M., Hogan, K. A., Mayer, L. A., Mix, A., Jennings, A., Stoner, J., Eriksson, B., Jerram, K., Mohammad, R., Pearce, C., Reilly, B., and Stranne, C.: The Holocene retreat dynamics and stability of Petermann Glacier in northwest Greenland, Nature Communications, 9, 2104, https://doi.org/10.1038/s41467-018-04573-2, number: 1 Publisher: Nature Publishing Group, 2018.

Jakobsson, M., Mayer, L. A., Nilsson, J., Stranne, C., Calder, B., O'Regan, M., Farrell, J. W., Cronin, T. M., Brüchert, V., Chawarski, J., Eriksson, B., Fredriksson, J., Gemery, L., Glueder, A., Holmes, F. A., Jerram, K., Kirchner, N., Mix, A., Muchowski, J., Prakash, A.,

725    Reilly, B., Thornton, B., Ulfsbo, A., Weidner, E., Åkesson, H., Handl, T., Ståhl, E., Boze, L.-G., Reed, S., West, G., and Padman, J.: Ryder Glacier in northwest Greenland is shielded from warm Atlantic water by a bathymetric sill, Communications Earth & Environment, 1, 45, https://doi.org/10.1038/s43247-020-00043-0, 2020.

Janssens, I. and Huybrechts, P.: The treatment of meltwater retention in mass-balance parameterizations of the Greenland ice sheet, Annals of Glaciology, 31, 133–140, https://doi.org/10.3189/172756400781819941, 2000.

730    Jennings, A. E., Hald, M., Smith, M., and Andrews, J. T.: Freshwater forcing from the Greenland Ice Sheet during the Younger Dryas: evidence from southeastern Greenland shelf cores, Quaternary Science Reviews, 25, 282–298, https://doi.org/10.1016/j.quascirev.2005.04.006, 2006.

Jennings, A. E., Sheldon, C., Cronin, T. M., Francus, P., Stoner, J., and Andrews, J.: The Holocene History of Nares Strait: Transition from Glacial Bay to Arctic-Atlantic Throughflow, Oceanography, 24, 26–41, https://www.jstor.org/stable/24861295, publisher: Oceanography
735    Society, 2011.

Jennings, A. E., Andrews, J. T., Oliver, B., Walczak, M., and Mix, A.: Retreat of the Smith Sound Ice Stream in the Early Holocene, Boreas, 48, 825–840, https://doi.org/10.1111/bor.12391, _eprint: https://onlinelibrary.wiley.com/doi/pdf/10.1111/bor.12391, 2019.

Joughin, I., B. Smith, I. H., and Scambos., T.: MEaSUREs multi-year greenland ice sheet velocity mosaic, version 1, https://doi.org/10.5067/QUA5Q9SVMSJG, 2016.

740    Joughin, I., Smith, B. E., and Howat, I. M.: A complete map of Greenland ice velocity derived from satellite data collected over 20 years, Journal of Glaciology, 64, 1–11, https://doi.org/10.1017/jog.2017.73, 2018.

Kajanto, K., Seroussi, H., de Fleurian, B., and Nisancioglu, K. H.: Present day Jakobshavn Isbræ (West Greenland) close to the Holocene minimum extent, Quaternary Science Reviews, 246, 106 492, https://doi.org/10.1016/j.quascirev.2020.106492, 2020.

Kajanto, K., Andresen, C., Seroussi, H., Rieckh, T., Briner, J. P., de Fleurian, B., Born, A., and Nisancioglu, K.: Holocene warmth explains the
745    Little Ice Age advance of Sermeq Kujalleq, Quaternary Science Reviews, 341, 108 840, https://doi.org/10.1016/j.quascirev.2024.108840, 2024.

Kaufman, D. S. and Broadman, E.: Revisiting the Holocene global temperature conundrum, Nature, 614, 425–435, https://doi.org/10.1038/s41586-022-05536-w, publisher: Nature Publishing Group, 2023.

Kelly, M. and Bennike, O.: Quaternary geology of western and central North Greenland, Rapport Grønlands Geologiske Undersøgelse, 153,
750    1–34, https://doi.org/10.34194/rapggu.v153.8164, 1992.

Khazendar, A., Fenty, I. G., Carroll, D., Gardner, A., Lee, C. M., Fukumori, I., Wang, O., Zhang, H., Seroussi, H., Moller, D., Noël, B. P. Y., van den Broeke, M. R., Dinardo, S., and Willis, J.: Interruption of two decades of Jakobshavn Isbrae acceleration and thinning as regional ocean cools, Nature Geoscience, 12, 277–283, https://doi.org/10.1038/s41561-019-0329-3, 2019.

Kjær, K. H., Bjørk, A. A., Kjeldsen, K. K., Hansen, E. S., Andresen, C. S., Siggaard-Andersen, M.-L., Khan, S. A., Søndergaard, A. S.,
755    Colgan, W., Schomacker, A., Woodroffe, S., Funder, S., Rouillard, A., Jensen, J. F., and Larsen, N. K.: Glacier response to the Little Ice Age during the Neoglacial cooling in Greenland, Earth-Science Reviews, 227, 103 984, https://doi.org/10.1016/j.earscirev.2022.103984, 2022.

Koch, L.: Contributions to the glaciology of north greenland, Meddelelser om Grønland, 65, 181–464, https://books.google.se/books?id=u84kzwEACAAJ, 1928.

760    Larour, E., Seroussi, H., Morlighem, M., and Rignot, E.: Continental scale, high order, high spatial resolution, ice sheet modeling using the Ice Sheet System Model (ISSM), Journal of Geophysical Research: Earth Surface, 117, https://doi.org/10.1029/2011JF002140, _eprint: https://onlinelibrary.wiley.com/doi/pdf/10.1029/2011JF002140, 2012.

Larsen, N. K., Kjær, K. H., Funder, S., Möller, P., van der Meer, J. J. M., Schomacker, A., Linge, H., and Darby, D. A.: Late Quaternary glaciation history of northernmost Greenland – Evidence of shelf-based ice, Quaternary Science Reviews, 29, 3399–3414, https://doi.org/10.1016/j.quascirev.2010.07.027, 2010.

Larsen, N. K., Funder, S., Linge, H., Möller, P., Schomacker, A., Fabel, D., Xu, S., and Kjær, K. H.: A Younger Dryas re-advance of local glaciers in north Greenland, Quaternary Science Reviews, 147, 47–58, https://doi.org/10.1016/j.quascirev.2015.10.036, 2016.

Larsen, N. K., Levy, L. B., Strunk, A., Søndergaard, A. S., Olsen, J., and Lauridsen, T. L.: Local ice caps in Finderup Land, North Greenland, survived the Holocene Thermal Maximum, Boreas, 48, 551–562, https://doi.org/10.1111/bor.12384, _eprint: https://onlinelibrary.wiley.com/doi/pdf/10.1111/bor.12384, 2019.

Lecavalier, B. S., Milne, G. A., Simpson, M. J. R., Wake, L., Huybrechts, P., Tarasov, L., Kjeldsen, K. K., Funder, S., Long, A. J., Woodroffe, S., Dyke, A. S., and Larsen, N. K.: A model of Greenland ice sheet deglaciation constrained by observations of relative sea level and ice extent, Quaternary Science Reviews, 102, 54–84, https://doi.org/10.1016/j.quascirev.2014.07.018, 2014.

Leger, T. P. M., Clark, C. D., Huynh, C., Jones, S., Ely, J. C., Bradley, S. L., Diemont, C., and Hughes, A. L. C.: A Greenland-wide empirical reconstruction of paleo ice-sheet retreat informed by ice extent markers: PaleoGrIS version 1.0, Climate of the Past Discussions, pp. 1–97, https://doi.org/10.5194/cp-2023-60, publisher: Copernicus GmbH, 2023.

Liu, Z., Otto-Bliesner, B. L., He, F., Brady, E. C., Tomas, R., Clark, P. U., Carlson, A. E., Lynch-Stieglitz, J., Curry, W., Brook, E., Erickson, D., Jacob, R., Kutzbach, J., and Cheng, J.: Transient Simulation of Last Deglaciation with a New Mechanism for Bølling-Allerød Warming, Science, 325, 310–314, https://doi.org/10.1126/science.1171041, publisher: American Association for the Advancement of Science, 2009.

MacGregor, J. A., Fahnestock, M. A., Colgan, W. T., Larsen, N. K., Kjeldsen, K. K., and Welker, J. M.: The age of surface-exposed ice along the northern margin of the Greenland Ice Sheet, Journal of Glaciology, 66, 667–684, https://doi.org/10.1017/jog.2020.62, 2020.

McIlhattan, E. A., Pettersen, C., Wood, N. B., and L'Ecuyer, T. S.: Satellite observations of snowfall regimes over the Greenland Ice Sheet, The Cryosphere, 14, 4379–4404, https://doi.org/10.5194/tc-14-4379-2020, publisher: Copernicus GmbH, 2020.

Millan, R., Rignot, E., Mouginot, J., Wood, M., Bjørk, A. A., and Morlighem, M.: Vulnerability of Southeast Greenland Glaciers to Warm Atlantic Water From Operation IceBridge and Ocean Melting Greenland Data, Geophysical Research Letters, 45, 2688–2696, https://doi.org/10.1002/2017GL076561, 2018.

Millan, R., Jager, E., Mouginot, J., Wood, M. H., Larsen, S. H., Mathiot, P., Jourdain, N. C., and Bjørk, A.: Rapid disintegration and weakening of ice shelves in North Greenland, Nature Communications, 14, 6914, https://doi.org/10.1038/s41467-023-42198-2, number: 1 Publisher: Nature Publishing Group, 2023.

Morlighem, M., Rignot, E., Seroussi, H., Larour, E., Ben Dhia, H., and Aubry, D.: Spatial patterns of basal drag inferred using control methods from a full-Stokes and simpler models for Pine Island Glacier, West Antarctica, Geophysical Research Letters, 37, 2010GL043 853, https://doi.org/10.1029/2010GL043853, 2010.

Morlighem, M., Seroussi, H., Larour, E., and Rignot, E.: Inversion of basal friction in Antarctica using exact and incomplete adjoints of a higher-order model, Journal of Geophysical Research: Earth Surface, 118, 1746–1753, https://doi.org/10.1002/jgrf.20125, 2013.

Morlighem, M., Bondzio, J., Seroussi, H., Rignot, E., Larour, E., Humbert, A., and Rebuffi, S.: Modeling of Store Gletscher's calving dynamics, West Greenland, in response to ocean thermal forcing, Geophysical Research Letters, 43, 2659–2666, https://doi.org/10.1002/2016GL067695, 2016.

Morlighem, M., Williams, C. N., Rignot, E., An, L., Arndt, J. E., Bamber, J. L., Catania, G., Chauché, N., Dowdeswell, J. A., Dorschel, B., Fenty, I., Hogan, K., Howat, I., Hubbard, A., Jakobsson, M., Jordan, T. M., Kjeldsen, K. K., Millan, R., Mayer, L., Mouginot, J., Noël, B. P. Y., O'Cofaigh, C., Palmer, S., Rysgaard, S., Seroussi, H., Siegert, M. J., Slabon, P., Straneo, F., van den Broeke, M. R.,

Weinrebe, W., Wood, M., and Zinglersen, K. B.: BedMachine v3: Complete Bed Topography and Ocean Bathymetry Mapping of Greenland From Multibeam Echo Sounding Combined With Mass Conservation, Geophysical Research Letters, 44, 11,051–11,061, https://doi.org/10.1002/2017GL074954, 2017.

Morlighem, M., Williams, C. N., Rignot, E., An, L., Arndt, J. E., Bamber, J. L., Catania, G., Chauché, N., Dowdeswell, J. A., Dorschel, B., Fenty, I., Hogan, K., Howat, I., Hubbard, A., Jakobsson, M., Jordan, T. M., Kjeldsen, K. K., Millan, R., Mayer, L., Mouginot, J., Noël, B. P. Y., O'Cofaigh, C., Palmer, S., Rysgaard, S., Seroussi, H., Siegert, M. J., Slabon, P., Straneo, F., van den Broeke, M. R., Weinrebe, W., Wood, M., and Zinglersen, K. B.: IceBridge BedMachine Greenland, Version 5, https://doi.org/10.5067/GMEVBWFLWA7X, 2022.

Mouginot, J. and Rignot, E.: Glacier catchments/basins for the Greenland Ice Sheet, https://doi.org/10.7280/D1WT11, 2019.

Mouginot, J., Rignot, E., Bjork, A. A., Broeke, M. v. d., Millan, R., Morlighem, M., Noel, B., Scheuchl, B., and Wood, M.: Forty-six years of Greenland Ice Sheet mass balance from 1972 to 2018, Proceedings of the National Academy of Sciences, 116, 9239–9244, https://doi.org/10.1073/pnas.1904242116, 2019.

Möller, P., Larsen, N. K., Kjær, K. H., Funder, S., Schomacker, A., Linge, H., and Fabel, D.: Early to middle Holocene valley glaciations on northernmost Greenland, Quaternary Science Reviews, 29, 3379–3398, https://doi.org/10.1016/j.quascirev.2010.06.044, 2010.

Nilsson, J., Van Dongen, E., Jakobsson, M., O'Regan, M., and Stranne, C.: Hydraulic suppression of basal glacier melt in sill fjords, The Cryosphere, 17, 2455–2476, https://doi.org/10.5194/tc-17-2455-2023, 2023.

Noël, B., van de Berg, W. J., Lhermitte, S., and van den Broeke, M. R.: Rapid ablation zone expansion amplifies north Greenland mass loss, Science Advances, 5, eaaw0123, https://doi.org/10.1126/sciadv.aaw0123, 2019.

O'Regan, M., Cronin, T. M., Reilly, B., Alstrup, A. K. O., Gemery, L., Golub, A., Mayer, L. A., Morlighem, M., Moros, M., Munk, O. L., Nilsson, J., Pearce, C., Detlef, H., Stranne, C., Vermassen, F., West, G., and Jakobsson, M.: The Holocene dynamics of Ryder Glacier and ice tongue in north Greenland, The Cryosphere, 15, 4073–4097, https://doi.org/10.5194/tc-15-4073-2021, publisher: Copernicus GmbH, 2021.

Otosaka, I. N., Shepherd, A., Ivins, E. R., Schlegel, N.-J., Amory, C., van den Broeke, M. R., Horwath, M., Joughin, I., King, M. D., Krinner, G., Nowicki, S., Payne, A. J., Rignot, E., Scambos, T., Simon, K. M., Smith, B. E., Sørensen, L. S., Velicogna, I., Whitehouse, P. L., A, G., Agosta, C., Ahlstrøm, A. P., Blazquez, A., Colgan, W., Engdahl, M. E., Fettweis, X., Forsberg, R., Gallée, H., Gardner, A., Gilbert, L., Gourmelen, N., Groh, A., Gunter, B. C., Harig, C., Helm, V., Khan, S. A., Kittel, C., Konrad, H., Langen, P. L., Lecavalier, B. S., Liang, C.-C., Loomis, B. D., McMillan, M., Melini, D., Mernild, S. H., Mottram, R., Mouginot, J., Nilsson, J., Noël, B., Pattle, M. E., Peltier, W. R., Pie, N., Roca, M., Sasgen, I., Save, H. V., Seo, K.-W., Scheuchl, B., Schrama, E. J. O., Schröder, L., Simonsen, S. B., Slater, T., Spada, G., Sutterley, T. C., Vishwakarma, B. D., van Wessem, J. M., Wiese, D., van der Wal, W., and Wouters, B.: Mass balance of the Greenland and Antarctic ice sheets from 1992 to 2020, Earth System Science Data, 15, 1597–1616, https://doi.org/10.5194/essd-15-1597-2023, publisher: Copernicus GmbH, 2023.

Otto, J., Holmes, F. A., and Kirchner, N.: Supraglacial lake expansion, intensified lake drainage frequency, and first observation of coupled lake drainage, during 1985–2020 at Ryder Glacier, Northern Greenland, Frontiers in Earth Science, 10, https://doi.org/10.3389/feart.2022.978137, publisher: Frontiers, 2022.

Pados-Dibattista, T., Pearce, C., Detlef, H., Bendtsen, J., and Seidenkrantz, M.-S.: Holocene palaeoceanography of the Northeast Greenland shelf, Climate of the Past, 18, 103–127, https://doi.org/10.5194/cp-18-103-2022, publisher: Copernicus GmbH, 2022.

Pattyn, F.: A new three-dimensional higher-order thermomechanical ice sheet model: Basic sensitivity, ice stream development, and ice flow across subglacial lakes, Journal of Geophysical Research, 108, https://doi.org/10.1029/2002JB002329, 2003.

Plach, A., Nisancioglu, K. H., Le clec'h, S., Born, A., Langebroek, P. M., Guo, C., Imhof, M., and Stocker, T. F.: Eemian Greenland SMB strongly sensitive to model choice, Climate of the Past, 14, 1463–1485, https://doi.org/10.5194/cp-14-1463-2018, publisher: Copernicus GmbH, 2018.

Reilly, B. T., Stoner, J. S., Mix, A. C., Walczak, M. H., Jennings, A., Jakobsson, M., Dyke, L., Glueder, A., Nicholls, K., Hogan, K. A., Mayer, L. A., Hatfield, R. G., Albert, S., Marcott, S., Fallon, S., and Cheseby, M.: Holocene break-up and reestablishment of the Petermann Ice Tongue, Northwest Greenland, Quaternary Science Reviews, 218, 322–342, https://doi.org/10.1016/j.quascirev.2019.06.023, 2019.

Seroussi, H. and Morlighem, M.: Representation of basal melting at the grounding line in ice flow models, The Cryosphere, 12, 3085–3096, https://doi.org/10.5194/tc-12-3085-2018, publisher: Copernicus GmbH, 2018.

Shapiro, N. M. and Ritzwoller, M. H.: Inferring surface heat flux distributions guided by a global seismic model: particular application to Antarctica, Earth and Planetary Science Letters, 223, 213–224, https://doi.org/10.1016/j.epsl.2004.04.011, 2004.

Simpson, M. J. R., Milne, G. A., Huybrechts, P., and Long, A. J.: Calibrating a glaciological model of the Greenland ice sheet from the Last Glacial Maximum to present-day using field observations of relative sea level and ice extent, Quaternary Science Reviews, 28, 1631–1657, https://doi.org/10.1016/j.quascirev.2009.03.004, 2009.

Slater, D. A. and Straneo, F.: Submarine melting of glaciers in Greenland amplified by atmospheric warming, Nature Geoscience, 15, 794–799, https://doi.org/10.1038/s41561-022-01035-9, publisher: Nature Publishing Group, 2022.

Smith, J. A., Callard, L., Bentley, M. J., Jamieson, S. S. R., Sánchez-Montes, M. L., Lane, T. P., Lloyd, J. M., McClymont, E. L., Darvill, C. M., Rea, B. R., O'Cofaigh, C., Gulliver, P., Ehrmann, W., Jones, R. S., and Roberts, D. H.: Holocene history of the 79N ice shelf reconstructed from epishelf lake and uplifted glaciomarine sediments, The Cryosphere, 17, 1247–1270, https://doi.org/10.5194/tc-17-1247-2023, publisher: Copernicus GmbH, 2023.

Tabone, I., Robinson, A., Montoya, M., and Alvarez-Solas, J.: Holocene thinning in central Greenland controlled by the Northeast Greenland Ice Stream, Nature Communications, 15, 6434, https://doi.org/10.1038/s41467-024-50772-5, publisher: Nature Publishing Group, 2024.

Tarasov, L. and Peltier, W. R.: Impact of thermomechanical ice sheet coupling on a model of the 100 kyr ice age cycle, Journal of Geophysical Research: Atmospheres, 104, 9517–9545, https://doi.org/10.1029/1998JD200120, _eprint: https://onlinelibrary.wiley.com/doi/pdf/10.1029/1998JD200120, 1999.

Thomas, E. K., Briner, J. P., Ryan-Henry, J. J., and Huang, Y.: A major increase in winter snowfall during the middle Holocene on western Greenland caused by reduced sea ice in Baffin Bay and the Labrador Sea, Geophysical Research Letters, 43, 5302–5308, https://doi.org/10.1002/2016GL068513, 2016.

Wangner, D. J., Jennings, A. E., Vermassen, F., Dyke, L. M., Hogan, K. A., Schmidt, S., Kjær, K. H., Knudsen, M. F., and Andresen, C. S.: A 2000-year record of ocean influence on Jakobshavn Isbræ calving activity, based on marine sediment cores, The Holocene, 28, 1731–1744, https://doi.org/10.1177/0959683618788701, publisher: SAGE Publications Ltd, 2018.

Weidick, A.: Comments on radiocarbon dates from northern Greenland made during 1977, Rapport Grønlands Geologiske Undersøgelse, 90, 124–128, https://doi.org/10.34194/rapggu.v90.7610, 1978.

Wilner, J. A., Morlighem, M., and Cheng, G.: Evaluation of four calving laws for Antarctic ice shelves, The Cryosphere, 17, 4889–4901, https://doi.org/10.5194/tc-17-4889-2023, publisher: Copernicus GmbH, 2023.

Wilson, N., Straneo, F., and Heimbach, P.: Satellite-derived submarine melt rates and mass balance (2011–2015) for Greenland's largest remaining ice tongues, The Cryosphere, 11, 2773–2782, https://doi.org/10.5194/tc-11-2773-2017, publisher: Copernicus GmbH, 2017.

Wiskandt, J., Koszalka, I. M., and Nilsson, J.: Basal melt rates and ocean circulation under the Ryder Glacier ice tongue and their response to climate warming: a high-resolution modelling study, The Cryosphere, 17, 2755–2777, https://doi.org/10.5194/tc-17-2755-2023, publisher: Copernicus GmbH, 2023.

Young, N. E., Lesnek, A. J., Cuzzone, J. K., Briner, J. P., Badgeley, J. A., Balter-Kennedy, A., Graham, B. L., Cluett, A., Lamp, J. L., Schwartz, R., Tuna, T., Bard, E., Caffee, M. W., Zimmerman, S. R. H., and Schaefer, J. M.: In situ cosmogenic $^{10}$Be–$^{14}$C–$^{26}$Al measurements from recently deglaciated bedrock as a new tool to decipher changes in Greenland Ice Sheet size, Climate of the Past, 17, 419–450, https://doi.org/10.5194/cp-17-419-2021, publisher: Copernicus GmbH, 2021.

Zeising, O., Neckel, N., Dörr, N., Helm, V., Steinhage, D., Timmermann, R., and Humbert, A.: Extreme melting at Greenland's largest floating ice tongue, The Cryosphere, 18, 1333–1357, https://doi.org/10.5194/tc-18-1333-2024, publisher: Copernicus GmbH, 2024.

Zekollari, H., Lecavalier, B. S., and Huybrechts, P.: Holocene evolution of Hans Tausen Iskappe (Greenland) and implications for the palaeo-climatic evolution of the high Arctic, Quaternary Science Reviews, 168, 182–193, https://doi.org/10.1016/j.quascirev.2017.05.010, 2017.

Åkesson, H., Morlighem, M., Nisancioglu, K. H., Svendsen, J. I., and Mangerud, J.: Atmosphere-driven ice sheet mass loss paced by topography: Insights from modelling the south-western Scandinavian Ice Sheet, Quaternary Science Reviews, 195, 32–47, https://doi.org/10.1016/j.quascirev.2018.07.004, 2018a.

Åkesson, H., Nisancioglu, K. H., and Nick, F. M.: Impact of Fjord Geometry on Grounding Line Stability, Frontiers in Earth Science, 6, https://doi.org/10.3389/feart.2018.00071, publisher: Frontiers, 2018b.

Åkesson, H., Morlighem, M., Nilsson, J., Stranne, C., and Jakobsson, M.: Petermann ice shelf may not recover after a future breakup, Nature Communications, 13, https://doi.org/10.1038/s41467-022-29529-5, 2022.